Atmos. Meas. Tech. Discuss., 4, 7277–7335, 2011
www.atmos-meas-tech-discuss.net/4/7277/2011/
doi:10.5194/amtd-4-7277-2011

Atmospheric Measurement Techniques Discussions

Determination of optical and microphysical properties of thin warm clouds using ground based hyper-spectral analysis

E. Hirsch[1], E. Agassi[2], and I. Koren[1]

[1]Department of Environmental Sciences, Weizmann Institute, Rehovot 76100, Israel
[2]Department of Environmental Physics, Israel Institute for Biological Research, Nes-Ziona, 74100, Israel

Received: 2 November 2011 – Accepted: 2 December 2011 – Published: 12 December 2011

Correspondence to: E. Hirsch (eitan.hirsch@weizmann.ac.il)

Published by Copernicus Publications on behalf of the European Geosciences Union.

Abstract

Clouds play a critical role in the Earth's radiative budget as they modulate the atmosphere by reflecting shortwave solar radiation and absorbing long wave IR radiation emitted by the Earth's surface. Although extensively studied for decades, cloud modelling in global circulation models is far from adequate, mostly due to insufficient spatial resolution of the circulation models. In addition, measurements of cloud properties still need improvement, since the vast majority of remote sensing techniques are focused in relatively large, thick clouds. In this study, we utilize ground based hyperspectral measurements and analysis to explore very thin water clouds. These clouds are characterized by liquid water path (LWP) that spans from as high as $\sim$50 g m^{-2} and down to 65 mg m^{-2} with a minimum of about 0.01 visible optical depth. The retrieval methodology relies on three elements: a detailed radiative transfer calculations in the longwave IR regime, signal enhancement by subtraction of a clear sky reference, and spectral matching method which exploits fine spectral differences between water droplets of different radii. A detailed description of the theoretical basis for the retrieval technique is provided along with a comprehensive discussion regarding its limitations. The proposed methodology was validated in a controlled experiment where artificial clouds were sprayed and their effective radii were both measured and retrieved simultaneously. This methodology can be used in several ways: (1) the frequency and optical properties of very thin water clouds can be studied more precisely in order to evaluate their total radiative forcing on the Earth's radiation budget. (2) The unique optical properties of the inter-region between clouds (clouds' "twilight zone") can be studied in order to more rigorously understanding of the governing physical processes which dominate this region. (3) Since the optical thickness of a developed cloud gradually decreases towards its edges, the proposed methodology can be used to study the spatial microphysical behaviour of these edges. (4) A spatial-temporal analysis can be used to study mixing processes in clouds' entrainment zone.

AMTD

4, 7277–7335, 2011

1 Introduction

Clouds play a critical role in the Earth's radiative budget as they modulate the atmosphere by reflecting shortwave solar radiation and absorbing longwave IR (LWIR) radiation emitted by the Earth's surface (Ramanathan et al., 1989). The radiative forcing of a single cloud depends on its height, thickness, and optical properties (Trenberth et al., 2009), and their accumulated effect depends on their lifetime, global coverage, and frequency of occurrence (Wylie et al., 2005). Shallow clouds are usually considered to have a net negative radiative forcing (cooling effect) as they reflect a substantial amount of the received solar irradiance while they have a minor effect on the total thermal radiation emitted by the Earth, since the magnitude of their emitted radiation is comparable with a cloud free surface. On the other hand, high clouds, such as anvils (Koren et al., 2010) or cirrus, might have a positive radiative forcing, since they have a relatively low reflectance in the visible portion of the spectrum, while the thermal contrast between them and the Earth is large. The effect of clouds on the Earth's radiative budget is so profound, that it has been shown that an increase of 15–20 % in the amount of low clouds could balance the expected heating effect of doubling the CO_2 concentration in the atmosphere (Slingo, 1990).

Although extensively studied for decades, cloud modelling in global circulation models (GCM) is far from adequate (Tselioudis and Jakob, 2002), mostly due to insufficient spatial resolution of the circulation models, which results in poor representation of the small scale microphysical processes that control clouds' properties (Heintzenberg and Charlson, 2009). Furthermore, cloud sensing techniques also need improvement (Turner et al., 2007), since most of the techniques which have been developed are oriented to relatively thick clouds that can be easily observed from space-borne platforms. Over the years, numerous algorithms have been suggested to retrieve clouds' properties by remote sensing measurements. These algorithms exploit radiative information in wavelengths from nanometeres to millimeters and can be characterized by the observation point – space or ground based measurements, and by the sensing method – either active or passive.

AMTD
4, 7277–7335, 2011

Although different approaches have been proposed, all of these methods share one thing in common: they depend upon radiative (e.g. optical thickness and albedo) and microphysical (e.g. droplet size distribution and thermodynamic phase) properties of the clouds. The theoretical basis for determining the optical thickness and effective radius of clouds by using reflected solar radiation was introduced by Nakajima and King (1990). Later, the Special Sensor Microwave/Imager (SSM/I) was used to retrieve liquid water content of clouds over the ocean (Weng and Grody, 1994). In addition, it was suggested that clouds liquid water and temperature could be derived by using an array of ground based devices, namely, microwave radiometer, ceilometer, radio acoustic sounding system and various surface meteorological instruments (Han and Westwater, 1995). The utility of space-borne multispectral passive remote sensing for retrieval of optical and microphysical properties for numerous cloud types was demonstrated (King et al., 1997). On the other hand, ground based cloud radars were used to retrieve the droplets effective radius profile of stratus clouds, by analyzing the radar reflectivity under various assumptions regarding the total number of droplets in the clouds (Frisch et al., 2002). More recently, the passive MODIS Airborne Simulator (MAS) was used to extract cloud properties even over snow and icy backgrounds (King et al., 2004). A noteworthy method to retrieve thin cloud's properties was presented by Turner (2005), who utilized ground based IR high spectral resolution measurements to retrieve mixed-phase cloud properties. The method successfully obtained the properties of simulated and measured thin water clouds with visible optical depths in the range of 0.2–4. The retrieval is based on an optimal estimation approach to fit a measured spectrum to a spectral database that was created by a radiation transfer model. This spectral analysis paradigm, is widely used in retrieval algorithms which exploit multispectral analysis.

As stated above, the main interest of the majority of the remote sensing techniques are relatively large, optically thick clouds. However, Turner et al. (2007) have overviewed the importance of thin liquid water clouds and the challenge in correctly retrieving their properties. In their work, they have defined thin clouds as clouds with

AMTD
4, 7277–7335, 2011

liquid water path (LWP) up to 100 g m^{-2} and have compared the performance of almost 20 different algorithms in retrieving the properties of a single layer, overcast, stratocumulus cloud field. The remote sensing techniques considered were wide ranging and spanned from the visible to the microwave portion of the spectrum; from ground based to space borne; both passive and active. The authors' main conclusion was that huge discrepancies exist among the different algorithms (even among algorithms that are in the same general classification), and that the cloud properties retrieval community should examine the accuracy of the algorithms when thin clouds are considered. An additional complexity to the challenges in correctly retrieving thin clouds properties arises from their expected occurrences. Koren et al. (2008) have studied the dependence of clouds' frequency (in a sparse cumulus cloud field) on their apparent size and showed that a power law governs the connection. This means that the number of clouds with a given area is proportional to the inverse of a^m, where a is the cloud area and m is the power exponent of the distribution ($1 < m < 2$). They concluded that the smallest detectable clouds may contribute significantly to the total cloud area as well as for the mean cloud field reflectance. This analysis coincides well with studies (Koren et al., 2007) which identified optically unique properties of the clouds' inter region (also known as "the clouds' twilight zone"). This region is characterized by a decrease in the apparent optical depth as the distance from the nearest detectable cloud increases. The precise nature of the "twilight zone" is still unclear, although several mechanisms have been suggested to explain its optical properties: undetected cloud fragments, aerosol humidification, and nearby scattering of solar radiation by clouds, are only some of the main suggested explanations. As most of the current retrieval methods are applied to space borne sensor data, thin warm clouds are usually ignored due to insufficient spatial and temporal resolution. In particular, the transition zone between clouds and clear skies is usually classified into one of two possible states: cloudy or clear. The purpose of our study is to introduce a new concept to determine and retrieve the properties of very thin warm clouds by using ground based IR spectral measurements. These kinds of measurements and analysis might shed light on some

AMTD
4, 7277–7335, 2011

of the most interesting enigmas of cloud microphysics and interaction with aerosols, and the clouds' effect on the radiative budget of the Earth.

In this study, we will utilize ground based infrared spectral analysis and measurements in order to explore very thin water clouds which are characterized by liquid water path that varies from as high as $50\,\mathrm{g\,m^{-2}}$ and down to $65\,\mathrm{mg\,m^{-2}}$ with a minimum of approximately 0.01 visible optical depth. The following section will introduce the theoretical basis for ground based passive sensing of the thermal IR spectrum of the zenith sky. The retrievals for the cloud effective radius and liquid water path (and the optical depth as a result) will be developed. The spectral differences in the extinction efficiencies of water droplets with different radii will be examined and the effect of these differences on the radiative transfer calculations will be discussed. We will show that thin liquid water clouds which contain varying liquid water paths and effective radii alter the magnitude and the spectrum of the down welling IR sky radiation. We will demonstrate how adequate spectral analysis can serve as a trigger for a mathematical best fit retrieval algorithm. This concept results in a standalone algorithm which first spectrally identifies the physical phenomenon which formed the measured signal, and only then is the optimal solution chosen in terms of mathematical best fit. The limitation of the proposed analysis, in terms of LWP and optical depth are discussed next in Sect. 3 by an overview of the methodology's sensitivity to fluctuations in the relative humidity field, atmospheric aerosols, and haze. Section 4 describes the experimental setup used to validate the proposed methodology. The main conclusions of these results and future work are discussed in detail in Sect. 5.

2 The down-welling radiance of the zenith sky in the presence of thin warm clouds in the long wave IR spectral band

In this section we will explore the theoretical basis for the spectral variability of the zenith sky radiance in the LWIR, in the presence of thin warm clouds. We will show that clouds which differ by their effective droplets radii alter the down-welling sky radiance in

AMTD
4, 7277–7335, 2011

a manner that can be identified by high spectral resolution measurements. Nevertheless, these spectral differences are small when compared to the clear sky background, and therefore a differential analysis technique is required in order to extract them from the clear sky background signature. As will be presented, this technique exploits the advantages of ground based, high temporal resolution measurements.

We will first explore how the obtained spectral properties of a single water droplet varies with its radius. Then a brief introduction to the analytical methods which have been used in this study is provided. Following that, we analyze the effect of thin monodisperse and polydisperse water clouds on the measured sky LWIR radiance. Finally, at the end of this section, we provide a detailed scheme of a retrieval method for the microphysical and the optical properties of very thin water clouds. This method is based on a spectral comparison between measured spectra and a spectral library created by radiative transfer calculations.

2.1 The spectral dependence of the extinction efficiency on the droplet's radius

The presence of water droplets in the atmosphere affects the magnitude and the spectrum of the LWIR sky radiation that reach the surface. The interaction of the radiation with the droplets is described by the generalized Mie theory (1908), which derives a wave equation with boundary conditions at the surface of a sphere by solving Maxwell's equations. The extinction, absorption, and scattering efficiencies are commonly characterized as a function of the size parameter (which is defined as $x = 2\pi r/\lambda$, where r is the droplet's radius and λ is the radiation wavelength). An alternative way to characterize the interaction of radiation and water droplets is to examine the mentioned efficiencies in a certain spectral region (e.g. the LWIR), for different droplets' radii. Such analysis reveals variations in the extinction efficiencies of droplets with different radii (Fig. 1). The refractive index of water (Palik, 1997), was used in order to calculate the extinction, absorption, and scattering efficiencies (Mätzler, 2002). The scattering coefficient is larger than the absorption coefficient (per unit length), therefore scattering is the dominant mechanism in which water attenuate the impinging LWIR radiation.

AMTD
4, 7277–7335, 2011

Apart from the evident differences in the magnitude of the extinction efficiency, one can notice how the extinction spectrum depends on the droplets radii. These spectral variations suggest that thin warm clouds with different droplets' effective radii might modify the down-welling sky radiance in distinct spectral forms. In the following subsections we will examine the latter hypothesis, by using a radiative transfer model which incorporates the optical properties of water clouds containing different water droplet size distributions.

2.2 Analysis methodology

The attempt to extract physical properties of remotely sensed objects is commonly referred to as solving an inverse problem. A typical approach to apply it, is composed of some forward model that predicts the expected signal under certain atmospheric parameters, and some mathematical curve fitting technique and threshold criteria to decide which atmospheric parameters present the most probable solution (Rodgers, 2000). As detailed hereafter, the presented methodology follows this general approach but with important modification prior to the stage of curve fitting technique. The presented approach treats thin warm clouds as semi transparent objects which alter the magnitude and the spectrum of the clear background signal. Therefore, we have used remote sensing techniques from the field of standoff detection and identification of gaseous and aerosols plumes, on the assumption that they are the most suitable tools to retrieve thin clouds' properties (see for example, Hirsch and Agassi, 2007; and Agassi et al., 2008).

The analysis presented in this study relies on 3 elements: a radiation transfer model, a method to extract the effect of a water cloud while eliminating the sky background, and a spectral matching method. A brief overview of each element is given in the following subsections.

AMTD
4, 7277–7335, 2011

2.2.1 Radiative transfer model

In this study, the PCModWin4.0 software, which includes the MODTRAN model (Berk et al., 1989), was used to predict the expected zenith sky radiance in the presence of various thin water clouds. MODTRAN is a radiation transfer model developed by the US Air Force Research Laboratory. It includes the HITRAN2000 database (Rothman et al., 2003) and it solves the radiative transfer equation including the effects of molecular and particulate absorption/emission and scattering, surface reflections and emission, solar/lunar illumination, and spherical refraction. The atmosphere is modeled as plane parallel (horizontally homogeneous), and its constituent profiles, both molecular and particulate, may be defined either using built-in models or by user-specified vertical profiles. The spectral range extends from the UV into the far-infrared and the user can define up to 4 aerosol types with distinct optical properties and incorporate each aerosol in the atmospheric column with specific extinction, absorption, and scattering coefficients. In our analysis, the MODTRAN input included the sounded atmospheric profile, the vertical extent of the cloud, and its water droplets' optical properties which were calculated for every simulated cloud.

2.2.2 Signal enhancement by sky background elimination

The presence of a thin water cloud alters the clear sky IR radiation. Unfortunately, as demonstrated in Sect. 2.3 below, the magnitude of the signal contributed only by the thin cloud is very small compared to the signal emerging from the clear sky itself. Therefore, in order to enhance the cloud's signature, we subtract the clear sky signal from the obtained spectra. The method of clear reference subtraction is commonly applied for detection and identification of weak gaseous plumes (Hirsch and Agassi, 2007). It enables retrieval of only the differential spectral signal, and therefore analyzes the phenomenon which created the signal without considering the background. This method is particularly advantageous for weak semi-transparent objects that otherwise

AMTD
4, 7277–7335, 2011

could not be analyzed, and in the following we will show how apparent similar spectra become spectrally distinctive when the clear sky reference is removed.

2.2.3 Spectral analysis

The process of subtracting the clear sky reference creates a differential spectrum. In order to classify the phenomenon which caused the differential signal, we assess its spectral similarity with a predicted set of library spectra which was pre-calculated. As commonly applied for identification of known reference spectra (Yuhas et al., 1992; Park et al., 2007), we have utilized the SAM – Spectral Angle Mapping (Kruse et al., 1993) analysis on the differential spectral signatures (Fig. 2). The SAM considers the spectral signals (each consisting of n wavelengths) as vectors in a n-dimensional space, and calculates the angle between two spectra as a measure of their similarity: distinct spectra will produce relatively large SAM values, while similar spectra will produce small values. The SAM metric is especially efficient when small spectral features are present, even though the complete spectral behaviour appears similar. Throughout this study, the SAM method has been applied on spectra which contained 16 wavelengths in the region of 8 µm–9 µm and 51 wavelengths in the region of 10 µm–13 µm. These wavelengths were chosen to match with the spectro-radiometer features used in our measurements (Sect. 4). The spectral region of 9 µm–10 µm was deliberately omitted since it contains the wide ozone absorption line (McCaa and Shaw, 1968), that might induce errors in the analysis.

2.3 The LWIR sky radiance in the presence of very thin warm monodisperse and polydisperse clouds

In this subsection we will investigate the spectral effect of very thin water clouds on the down welling IR radiance of the clear sky. Throughout this study we will use the atmospheric profile measured with a radiosonde in the Beit-Dagan station (Website: "Atmospheric Sounding"), on 8 August 2010, 12:00 UTC (Fig. 3), as an input for the

AMTD
4, 7277–7335, 2011

radiative transfer calculations. The Israeli summer is characterized by inactive weather and very stable meteorological conditions, therefore this atmospheric profile represents a typical Israeli daytime summer profile. According to the ceilometer readings in the Ben-Gurion airport (Website: "Station Observations"), which is located approximately 10 km from our measurement site, the average cloud base height was 792 m during the morning hours. Therefore, all the radiative transfer calculations simulated clouds at 800 m above the surface.

2.3.1 The effect of monodisperse water clouds on the LWIR sky radiance

The extinction coefficient per unit length of a monodisperse water cloud with a given liquid water content (LWC) is given by

$$\sigma_{\text{ext}}(\lambda) = N \pi r^2 Q_{\text{ext}}(\lambda, r) \tag{1}$$

where r is the droplet radius, and $Q_{\text{ext}}(\lambda, r)$ is the extinction efficiency of a single water droplet with radius r at wavelength λ. N is the droplet density (i.e. the number of droplets per unit volume) which equals the LWC divided by the mass of a droplet, i.e. $N = \text{LWC}/(4/3\, \pi r^3 \rho)$ (where ρ is the density of water, taken here in mks units as $1000\,\text{kg m}^{-3}$). Exactly the same formulation holds for deriving the absorption and scattering coefficients ($\sigma_{\text{abs}}(\lambda)$ and $\sigma_{\text{sct}}(\lambda)$, respectively) per unit length. These spectral coefficients are used to solve the radiative transfer equations in the presence of clouds.

A set of 50 m thick, monodisperse clouds with equal liquid water content of $15\,\text{mg m}^{-3}$, were simulated at equal heights and under the same atmospheric profile. The only difference between the clouds was the water droplet radius. The expected zenith sky LWIR radiances in the presence of the simulated clouds are presented (Fig. 4). The figure creates an impression that the anticipated spectra are quite similar, since most of the signal originates from the clear sky background. As explained above, subtraction of the clear reference eliminates the sky background and extracts the sole effect of the thin clouds (Fig. 5). The differential spectra appear quite distinct as small droplets attenuate more radiation in the 11 µm–13 µm region while large droplets

AMTD
4, 7277–7335, 2011

attenuate more radiation in the 8 µm–9 µm region. The use of the SAM index on the differential spectra (Fig. 6) quantifies the apparent spectral variations of the sky radiance in the presence of thin clouds. Three distinctive areas appear in the mutual cross SAM matrix of the differential spectra: (1) small water droplets with radii less than 2 µm have spectral signals which are relatively similar (low cross SAM values), while their spectra are distinct from water droplets with higher radii. (2) Medium size water droplets with radii of 2 µm–3 µm are different from water droplets with other radii. (3) Spectra of larger water droplets with radii greater than 4 µm appear spectrally different than smaller droplets, but the ability of the technique to distinguish between droplets in the region of 4 µm–10 µm is relatively low. These distinctive areas reinforce the hypothesis that spectral variations in the extinction efficiencies alter the radiation in a spectrally different manner, and that using the SAM on the differential spectral signatures might be useful to distinguish between clouds with different droplets' effective radii.

2.3.2 The effect of polydisperse water clouds on the LWIR zenith sky radiance

Clouds droplets are not monodisperse. The size distribution of water droplets of cumulus clouds has been extensively studied for several decades. A modified Gamma function was proposed to represent the density size distribution of clouds' droplets as a function of their radius (Deirmendjian, 1964). Specifically, the size distribution is given by

$$n(r) = a\, r^{\alpha}\, e^{-b\, r\, \gamma} \tag{2}$$

where $n(r)$ is the normalized size distribution, i.e. $\int_0^{\infty} n(r)\, dr = 1$, and a, α, b, and γ are positive constants. Utilizing the modified Gamma size distribution, we have created a large dataset of more than 120 000 size distributions of water droplets in order to cover a wide range of possible cases. The droplets size distributions which were used in our simulation (Table 1), represent typical distributions that were measured in natural low clouds (Miles et al., 2000). These simulated distributions span a 2-D space of effective radius (r_{eff}) and LWC (Fig. 7), which will later be used by MODTRAN to construct a

Discussion Paper | Discussion Paper | Discussion Paper | Discussion Paper |

AMTD

4, 7277–7335, 2011

Optical and microphysical properties of thin warm clouds

E. Hirsch et al.

Title Page
Abstract Introduction
Conclusions References
Tables Figures
◀| |▶
◀ ▶
Back Close
Full Screen / Esc
Printer-friendly Version
Interactive Discussion

spectral library of possible sky radiances in the presence of different water clouds. The effective radius is a commonly used parameter to represent the water droplets size distribution (Hansen and Travis, 1974). Specifically,

$$r_{\mathrm{eff}} = \frac{\int_0^\infty r^3\, n(r)\, dr}{\int_0^\infty r^2\, n(r)\, dr} \tag{3}$$

and it is related to the visible optical depth of the cloud (Stephens, 1994), by

$$\mathrm{OD_{vis}} = \frac{3\,\mathrm{LWP}}{2\,\rho\, r_{\mathrm{eff}}} \tag{4}$$

where LWP is the liquid water path in the cloud, namely $\mathrm{LWP} = \int_{h_{\mathrm{base}}}^{h_{\mathrm{top}}} \mathrm{LWC}(h)\, dh$.

It is worth noticing that the use of r_{eff} as a measure for the cloud optical depth is not valid in the IR region, as the original calculation of r_{eff} (Hansen and Travis, 1974), assumed the droplet radius is noticeably larger than the wavelength, which is valid only in the visible portion of the spectrum. Nevertheless, in order to follow conventional characterization of clouds in the scientific community, we will use the r_{eff} and $\mathrm{OD_{vis}}$ parameters to characterize the simulated and measured clouds.

In a similar manner to Eq. (1), the spectral extinction coefficient of a water cloud with a given droplet size distribution is

$$\sigma_{\mathrm{ext}}(\lambda) = N \int_0^\infty n(r)\, \pi\, r^2\, Q_{\mathrm{ext}}(\lambda, r)\, dr \tag{5}$$

where N is the total number of water droplets per unit volume, and $n(r)$ is a normalized size distribution as defined previously.

The same cross SAM analysis on the differential spectral signatures of polydisperse water clouds (Fig. 8) shows that the spectral variability still holds even when the droplets follow a modified Gamma distribution function. From the figure, it is obvious that clouds with small r_{eff} (less than 1 µm) are spectrally distinct, as their cross

Discussion Paper | Discussion Paper | Discussion Paper | Discussion Paper |
AMTD
4, 7277–7335, 2011
Optical and microphysical properties of thin warm clouds
E. Hirsch et al.

SAM values with other clouds are relatively high. In the same manner, clouds with medium effective radius ($1\,\mu m < r_{eff} < 2.75\,\mu m$) are easily distinguished by the SAM analysis. Clouds with $r_{eff} > 3$ appear relatively similar to each other, but quite different from clouds with smaller r_{eff}.

2.4 Retrieval methodology

Following the theoretical basis presented in the previous subsections, we propose the following methodology (Fig. 9), which is composed of 3 elements, for the retrieval of very thin liquid water clouds' microphysical and optical properties:

A. Simulating the expected IR spectral signature of the zenith sky in the presence of very thin liquid water clouds with various microphysical properties: the simulation should use a radiative transfer model, that considers effects of molecular and particulate emission and scattering, and create a large spectra database which will serve as a spectral library.

B. Continuous, ground based, measuring of the zenith sky: in order to analyze small scale dynamical processes within the clouds, measurement of the zenith sky with reasonable spectral, spatial, and temporal resolution is needed. The sensor's field of view (FOV) should not exceed several milliradians, which correspond to several square meters at the top of the boundary layer. The acquisition rate should be as high as possible in order to allow the retrieval of the temporal dynamics of the cloud, and the sensor's sensitivity should be high enough to extract the signal formed by the presence of the thin clouds. Regarding the required spectral resolution, the analysis presented in this study utilized 67 spectral bands. Nevertheless, it is possible that the spectral analysis can be performed with a relatively small number of narrow spectral bands, and as suggested in Sect. 3, even 5 spectral bands might be suitable to sustain the spectral variability between thin clouds.

AMTD
4, 7277–7335, 2011

C. Retrieving the microphysical and optical properties of a cloud whenever a substantial increase in the measured sky radiation occurs: using a spectral match index (SAM analysis for example) between the measured signal and the spectral library. This spectral analysis will serve as a trigger for the retrieval process by identifying that the source of the measured signal is indeed water droplets. The second stage is comparing the magnitude of the measured signal with the spectral library signals and choosing a set of possible solutions of liquid water path, effective radius, and optical depth of the cloud.

The results of utilizing the proposed methodology on measured data are presented in Sect. 4, where a controlled experiment was conducted in order to validate the proposed methodology.

3 Sensitivity analysis and induced bias or misclassification in the retrieved parameters

This section presents an analysis of the range of the optical and microphysical properties that can be retrieved by the proposed method. In addition, the method's sensitivity to the number of spectral bands and noise level is analyzed. Moreover, a detailed discussion regarding the bias or misclassification that can be induced as a result of fluctuations in the relative humidity, aerosols, and haze is presented.

3.1 Sensitivity analysis

In order to assess the method's range we need to use a specific atmospheric profile in our radiative transfer model and to consider the performance in terms of signal to noise ratio (SNR). As before, the atmospheric profile used for this analysis was measured during 8 August 2010 12:00 UTC in a nearby meteorological station (Website: "Atmospheric Sounding"). As presented in the following Sect. 4, a controlled experimental setup was used to validate the proposed method. Our main instrumental device

AMTD
4, 7277–7335, 2011

was the SR5000 (CI-Systems, Israel), a calibrated spectro-radiometer in the range of 2.5 µm–14 µm. The radiometer was calibrated with an extended area infrared source (SR80, CI-Systems, Israel), and the noise equivalent spectral radiance (NESR) level was measured in the lab, and it found to be $6.4 \times 10^{-6}\,\mathrm{W\,cm^{-2}\,str^{-1}\,\mu m^{-1}}$ for a wavelength of 10 µm. As detailed below, through our analysis a SNR threshold of 3 was applied.

Under the mentioned atmospheric profile (see Fig. 3), we used radiative transfer calculations to create a spectral library which included a total of 121 010 clouds. The clouds contained varying LWC, effective radius and thickness. In order to model realistic cases of thin clouds that can be measured by our sensors, we have filtered out some of the clouds from the spectral library. On one hand, as a cloud becomes thinner, its optical depth and its effect on the sky radiance diminishes. On the other hand, as a cloud becomes optically thicker, its apparent IR spectral signature approaches the emitted radiance of a blackbody at the same temperature as the air layer in which it resides (Yamamoto et al., 1970). At this limit, the proposed methodology cannot distinguish between signals that originate from thick clouds with different effective radii. As a result, as the simulated clouds gain optical depth, the spectral variability decreases gradually, until the point where almost no spectral variation exists whatsoever (Fig. 10).

Let S be the spectrum of the zenith sky in the presence of a thin cloud, and S_{sky} be the spectrum of the clear zenith sky. Generally, we consider only the clouds with a signal to noise ratio (SNR) larger than 3 in the wavelength of 10 µm (compared to the noise level of the SR5000 spectro-radiometer), but are still thin enough (i.e. their obtained signal is distinct from a blackbody spectrum). Specifically, we considered all the clouds which passed the following criteria: $S_{\lambda=10\,\mu\mathrm{m}} - S_{\mathrm{sky}\lambda=10\,\mu\mathrm{m}} > 3 \cdot \mathrm{NESR}_{\lambda=10\,\mu\mathrm{m}}$ and

$$\left.\frac{S - S_{\mathrm{sky}}}{S_{\mathrm{sky}}}\right|_{\lambda=10\,\mu\mathrm{m}} < 0.9 \cdot \max_{\mathrm{over\_all\_clouds}}\left(\left.\frac{S - S_{\mathrm{sky}}}{S_{\mathrm{sky}}}\right|_{\lambda=10\,\mu\mathrm{m}}\right) \tag{6}$$

AMTD
4, 7277–7335, 2011

Title Page
Abstract | Introduction
Conclusions | References
Tables | Figures
◂◂ | ▸▸
◂ | ▸
Back | Close
Full Screen / Esc
Printer-friendly Version
Interactive Discussion

The right hand side of the criteria ensures that we filter out all the thick clouds with spectral behaviour similar to a blackbody. The result of these screenings was a database consisting of 81 197 spectral signatures with varying parameters (see Table 2).

3.1.1 Method's sensitivity to instrumental noise level

As stated above, we used the SR5000 spectro-radiometer which has a noise level of $6.4 \times 10^{-6}\,\mathrm{W\,cm^{-2}\,str^{-1}\,\mu m^{-1}}$ for a wavelength of 10 µm, and a SNR threshold of 3 was applied. In this subsection we present a simple analysis that aims to quantify the possible influence of the noise level of the measuring device. For every differential signature in the spectral library we added a white noise that corresponds to SNR of 3, and calculated the spectral angle (SAM) between the original and noisy spectra. As detailed in Sect. 4, our analysis utilized a SAM threshold of 10° during the validation experiment. Therefore, we consider a differential spectrum to be affected by noise only when the SAM angle between the original and noisy spectra exceeds 5°. Our analysis indicates that the proposed methodology is quite robust, as clouds with LWC higher than $13.8\,\mathrm{mg\,m^{-3}}$ are not affected by the random noise.

3.1.2 Method's sensitivity to instrumental spectral features

Every spectro-radiometer suffers from inherent spectral features, and in this subsection we have analyzed the effect of such features in terms of possible misclassification of the proposed methodology. The analysis utilized the commonly used technique of PCA – principal component analysis (Johnson and Wichern, 1992) over a long time series of differential spectral signals which were measured in the laboratory. As stated previously, the proposed method utilizes 67 spectral bands, and therefore the PCA produced 67 eigenvectors. In order to examine whether the measuring device contains inherent spectral features that might induce bias to our methodology, we used the same analysis which is detailed previously to compare the spectral similarity between these

AMTD
4, 7277–7335, 2011

eigenvectors and the expected spectra of thin clouds at the spectral library which was produced by MODTRAN. The spectral angle (SAM) between every eigenvector and every cloud differential signal was calculated (Fig. 11). The red line in Fig. 11 is the total variance of every eigenvector (sorted in descending order as commonly presented in PCA analysis), and the blue line is the lowest (spectrally closest) SAM value between every corresponding eigenvector and the clouds spectral library. One can notice that the closest SAM value between any of the eigenvectors and the clouds signals stands on 46°, while the SAM threshold applied in our study is 10°. The analysis, along with the usage of a signal to noise ratio (SNR) threshold of 3 (in wavelength of 10 µm) on the measured signal, suggests that inherent noise and spectral features cannot affect our methodology.

3.1.3 Method's sensitivity to the number of spectral bands

As mentioned above, the SAM analysis utilized 67 spectral bands that are measured by the spectro-radiometer between 8 µm–13 µm. Due to practical and technical reasons, most developers of remote-sensing techniques prefer to use as low as possible number of spectral bands in their analysis. In light the above, a simple analysis was conducted to check whether the spectral variability holds when the number of spectral bands is reduced. Since it is practically impossible to check all the permutations of the original spectral bands, a simple bands reduction iterative scheme was applied. A single spectral band was eliminated in every iteration. The band that was chosen was the band that its absence gave the best cross SAM matrix. Where there might be several ways to define what is the best cross SAM matrix, we compared different matrices by the sum of their first diagonal. Large values indicate that the signatures largely differ from one another, whereas small values indicate the signatures are more spectrally similar. Our iterative procedure was applied until the number of bands was 5.

Figure 12 compares the cross SAM matrix using only 5 spectral bands to the original cross SAM matrix (67 bands). It clearly shows that the spectral variability still holds even when 5 bands are used. In spite these encouraging results, it should be noted

AMTD
4, 7277–7335, 2011

that a comprehensive analysis regarding the optimal number of bands should still be performed. Such analysis must consider more aspects of bands reduction, namely noise effect, misclassification, and possible biases.

3.2 Induced bias or misclassification as a result of fluctuations in the relative humidity, aerosols, and haze

The purpose of the proposed methodology is to extract the properties of water clouds with very small optical depth, by analyzing the spectrum and the magnitude of the signal. Fluctuations in relative humidity, aerosol loading, and haze are also characterized by small optical depths. Therefore, it is essential to examine whether such fluctuations and thin water clouds can alter the sky radiance in a similar way (in terms of spectrum and magnitude). If such similarities exist, the proposed method might falsely interpret such fluctuations as thin water clouds. In addition, when thin water clouds do exist in the sensor's FOV, fluctuations in water vapours and aerosols might induce bias to the retrieved parameters.

In this subsection we will analyze the zenith sky radiance in the presence of fluctuations in relative humidity, aerosols, and haze. The spectral change as well as the magnitude of the signal will be analyzed, and we will estimate or try to bound the bias that might be induced to the retrieved parameters as a result of such fluctuations.

3.2.1 Relative humidity

Water vapour molecules are a substantial constituent of the troposphere and are one of the key parameters which determine the measured thermal radiation of the sky. Although water vapours do not scatter the LWIR radiation, its absorption alters the down welling sky radiance. Therefore it is essential to verify that short term variations in the water vapour column distribution do not induce substantial changes in the sky radiance, compared to the changes induced by thin water clouds. At first, we used radiative transfer calculations to analyze the magnitude of the expected change in the sky radiance as a result of fluctuations in water vapour. Under the mentioned atmospheric profile, our modelling results predict that the expected change in the sky radiance at wavelength 10 µm is 1.52×10^{-5} W cm^{-2} str^{-1} µm^{-1} when the relative humidity in the layer of 800–850 m raises from 10 % to 100 %. This radiative difference is small since the total transmittance of a 50 m layer of water vapours at temperature of 26.23 °C (the air temperature of the layer in the chosen atmospheric profile) stands on 0.992 (therefore the layer emissivity is 0.008). It suggests that even such extreme and unlikely fluctuations are expected to create a change in the measured sky radiance smaller than our predefined SNR threshold (1.92×10^{-5} W cm^{-2} str^{-1} µm^{-1}, corresponding to 3 times the NESR of the SR5000), and therefore fluctuations in water vapour cannot be falsely interpreted as thin water clouds.

In addition, the bias that water vapour fluctuations might induce on the retrieved parameters, when thin clouds are present in the sensor's FOV was analyzed. In order to examine the influence of water vapour fluctuations on the spectral radiance of the simulated clouds, we used radiative transfer calculations to predict the sky spectrum in the presence of thin clouds with two different humidity profiles. The first profile was the true sounded atmospheric profile which was measured by the radiosonde and indicated a relative humidity of 32 % in the 50 m layer below the cloud base (750–800 m). The second profile differed by the relative humidity in the layer below the clouds, which was modified to 50 %. The spectral angle (in terms of SAM) between every two differential sky spectra was calculated, as presented in Fig. 13. As seen in the figure, only clouds which contained LWC lower than 4 mg m^{-3} might experience a spectral shift higher than 5°. We repeated this analysis by altering the relative humidity (in the 750–800 m layer) in the range of 10 %–100 %. The assessment of the relative humidity impact is shown in Fig. 14. For every relative humidity value in the 750 m–800 m layer, we analyzed the maximal LWC value for which clouds will experience a spectral shift higher than 5°. The main conclusion from this analysis is that even extreme and unlikely fluctuations in the relative humidity layer below the cloud, might affect clouds with LWC at most of 35 mg m^{-3}.

AMTD
4, 7277–7335, 2011

3.2.2 Aerosols

The origin of aerosols in the atmosphere is attributed to many sources and can be emitted by either natural processes or by anthropogenic activity (IPCC, 2007). The vast majority of these airborne particles are small compared to water droplets, and as a result their radiative effect is mostly noticeable in the visible portion of the spectrum. Nevertheless, measurements in the IR regime have been occasionally made. Aerosols' IR optical properties during the ACE-Asia campaign were measured (Markowicz et al., 2003), and it was shown that the mean aerosol optical depth at 10 µm was 0.08 (for the entire atmospheric column). Apart the complete optical depth, aerosol optical properties in the LWIR have been studied (Thomas et al., 2005; Richwine et al., 1995; Toon et al., 1976; Volz, 1972, 1973), and in addition, the effect of changes in the relative humidity on the extinction coefficients of atmospheric aerosols was presented (Nilsson, 1979). These properties can be incorporated in radiative transfer models in order to retrieve aerosols' radiative effect. MODTRAN offers several predefined aerosol models, and in this study we have analyzed the effect of the rural, maritime, and urban models which are here described briefly. The rural model represents the aerosol conditions in continental areas which are not directly influenced by urban and industrial aerosol sources. The rural aerosols are assumed to be composed of a mixture of 70 percent of water-soluble substances and 30 percent dust-like aerosols. The size distribution of this aerosol model is parameterized as the sum of two log-normal size distributions, to represent the multimodal nature of the atmospheric aerosols. In addition, the aerosol size is determined as a function of the humidity in the layer in which they are simulated. The urban aerosol model is a modification of the rural model by an addition of aerosols from combustion products and industrial sources. The mixture is composed of 80 percent rural aerosols and 20 percent sootlike aerosols. The maritime aerosol model largely differs from the previous models, and is composed of two components: aerosols developed from sea spray, and a continental component assumed identical to the rural aerosol with the exception that the very large particles were eliminated, since the will

AMTD
4, 7277–7335, 2011

eventually be lost due to fallout. These aerosol models are characterized by their optical properties in the visible and the LWIR region of the spectrum, and can be readily incorporated in MODTRAN in a certain atmospheric layer by specifying the aerosol's extinction coefficient for unit length at a wavelength of 550 nm.

To estimate the effect of aerosols on the retrieved methodology we used the mean aerosols optical thickness (AOT) that was measured in a local AERONET site (Holben et al., 1998; and Website: "Aerosol Robotic Network (AERONET) Homepage"). AERONET's average AOT during the months of August through October 2010 was 0.26 at 500 nm. We have assumed an extreme scenario where all the atmospheric aerosols are concentrated in a 50 m layer, thus MODTRAN's required input for extinction coefficient was calculated to be $\sigma(\lambda = 550\,\text{nm}) = 0.26/0.05 = 5.2\,\text{km}^{-1}$. It is important to note that such extreme extinction causes the optical visibility (defined as 2 % at wavelength of 550 nm) to be 752 m, and it is typical for heavy dust storms (during which, all the lower troposphere is filled with dust). Obviously, this assumption enhances the radiative effect of aerosols on the sky spectrum. The top left panel in Fig. 15 presents the expected differential spectrum in the presence of such aerosols in the atmospheric layer between 800 m to 850 m, using the atmospheric profile of 8 August 2010. One should compare the magnitude of the differential signals which are expected by a thin water cloud with LWC of $15\,\text{mg}\,\text{m}^{-3}$ (Fig. 5) and thick, dust-storm like aerosol layer (top left panel in Fig. 15). It is noticeable that even extreme, unrealistic aerosol condition which were simulated, are expected to produce a signal which is still an order of magnitude less that is expected for a thin water cloud.

To estimate the spectral effect of aerosols on the retrieved parameters, we calculated the SAM index between every aerosol model's differential spectrum and the simulated clouds' differential spectrum. The SAM angle values for the different aerosol models are presented in Fig. 15. It is notable that rural and maritime aerosols do not pose any significant spectral bias as the minimal (spectrally close) SAM angle between the aerosols and the clouds stands at 14.76° and 14.35° respectively. However, it seems that the presence of urban aerosols can affect the sky radiance in a way which is similar

AMTD
4, 7277–7335, 2011

to the effect of very thin clouds with $r_{eff} > 2\,\mu m$, since the minimal SAM angle between the urban aerosols and the clouds is 4.79°. Nevertheless, even in a scenario where all the aerosols are concentrated in a 50 m layer, and the optical properties of the layer resemble that of a dust storm, the magnitude of the differential spectrum caused by the urban aerosols is very low: only a 6 % increase in the radiance at wavelength of 10 µm compared to the clear sky signal. In any case, as described in Sect. 4.1, this increase represents a signal to noise ratio of 2 (compared to the measuring device) and we have discarded any signals with SNR lower than 3. This analysis shows that the influence of tropospheric aerosols is marginal for any practical purpose, and that their effect on the retrieved cloud parameters is negligible.

3.2.3 Haze

The growth of a water droplet due to condensation is well described by the Köhler curve (1936). The required ambient supersaturation needed to support spontaneous condensational growth of the droplet depends on the exact chemical composition of the solution droplet as well as on the droplet's radius. When the ambient supersaturation is high enough, the droplet can pass a thermodynamic barrier represented by the Köhler peak. Such a droplet is said to be activated and will continue to grow by condensation and become a cloud droplet. On the other hand, insufficient ambient supersaturation will cause a droplet to stay in stable equilibrium. Under these conditions, a slight increase in its size (by condensation) will cause immediate evaporation that will bring it back to the equilibrium size, and a slight decrease in its size (by evaporation) will result in condensation that will return its size. Such unactivated droplets are called haze droplets.

The proposed methodology presented in this study can distinguish between water droplets with different radii due to their optical properties, but it obviously cannot separate between different microphysical states. Nevertheless, the typical effective radius of haze cloud is 0.05 µm (Deirmendjian, 1964), yielding a volume extinction coefficient in the IR band, which is about 3 orders of magnitude smaller than that of a typical water cloud. These kind of haze clouds are expected to have a negligible effect on the obtained effective radius and optical depth of thin clouds. Therefore, we are quite confident to conclude that when the effective radius of a certain cloud is retrieved, it represents an activated water cloud rather than a haze cloud.

3.3 Sensitivity of the proposed method to variations in the atmospheric profile

The analysis presented in the former sections utilized a certain atmospheric profile which was measured in a nearby meteorological station on a specific day. In order to study the efficacy and applicability of the proposed method it is important to analyze its sensitivity to the temperature and humidity profile. Therefore, we picked 16 atmospheric profiles (Website: "Atmospheric Sounding"), which were measured simultaneously at different locations around the globe (Fig. 16), and repeated the analysis presented in Sect. 3.1 to create a spectral library of thin clouds for every measured profile.

Figure 17 presents the expected clear sky zenith radiance under the different atmospheric profiles. As expected, the radiance of the zenith sky is smaller under drier and colder atmospheric conditions, and noticeable variations exist in the clear sky spectrum, both in terms of the spectral shape and in the magnitude of the signal. As detailed in Sect. 2, the methodology relies on spectral analysis of the variability of the differential spectrum which is created by subtracting the clear sky signal from the zenith sky radiance in the presence of a thin cloud. Figure 18 presents the expected differential spectrum under the different atmospheric profiles in the presence of a thin warm cloud characterized by an effective radius of 2.1 µm and LWP of 750 mg m^{-2}. It is noticeable that the magnitude of the differential signal is comparable under all atmospheric profiles which suggests that in terms of signal to noise ratio, the proposed method can be used globally.

Nevertheless, examining Fig. 17 reveals spectral variability that exists for the same cloud under different atmospheric profiles. Quantifying this spectral variability in terms of SAM (Fig. 19) provides interesting insights on the applicability of the proposed method: clouds under similar atmospheric conditions will have small cross SAM values (i.e. their spectral signatures will resemble each other), whereas clouds under extremely different atmospheric profiles can differ from each other by a cross SAM value of up to $\sim 30°$.

The analysis presented in this subsection suggests that the proposed methodology is applicable for global use under wide range of seasonal, diurnal, and meteorological conditions. Nevertheless, the analysis emphasizes that adequate characterization of the observing system is necessary in order to retrieve valid and trustable results, and one must rely on measured representative atmospheric profile (in terms of general location and season) and trustable radiative transfer model that can incorporate user-defined profiles.

4 Validation of the proposed methodology in a controlled environment experiment

In order to validate the proposed methodology, a controlled experiment was conducted outdoors (Fig. 20). The purpose of this small-scale experiment was to validate the main concept that stands in the basis of the proposed methodology, namely that usage of a radiative transfer model combined with spectral analysis allows for the retrieval of cloud water droplet effective radius (assuming the type of the droplets size distribution is known). An artificial water cloud was sprayed with an air-atomizing nozzle, and the cloud's droplets size distribution was varied by altering the air pressure supplied to the nozzle. Our main instrumental device was the SR5000 (CI-Systems, Israel), a calibrated spectro-radiometer in the range of 2.5 µm–14 µm, which measures the incident radiance with a circular variable filter (CVF). The radiometer was calibrated with an extended area infrared source (SR80, CI-Systems, Israel), thus its output was provided in radiance ($\mathrm{W\,cm^{-2}\,str^{-1}\,\mu m^{-1}}$). We placed the SR5000 below the passing cloud, pointed it to the zenith, and operated it in a single mode: the FOV was selected to 6 mrad and an acquisition rate of 5 Hz was applied. In addition to the SR5000, a thermal

AMTD
4, 7277–7335, 2011

imager (A40, FLIR SYSTEMS, USA) was used in order to continuously acquire images of the zenith sky and artificial cloud. This broadband (7–14 µm) IR imager is based on an uncooled microbolometer sensor with 240 × 320 pixels, calibrated to effective radiant temperature. It has a wide FOV (18° × 24°, equivalent to 314 mrad × 419 mrad) and its acquisition rate was set to 6.25 Hz. Complementary to the on-site measurement assembly, we used the atmospheric profile which was measured in the meteorological station in Beit-Dagan (Website: “Atmospheric Sounding”), located approximately 10km from our measurement site. This atmospheric profile was used as an input for the radiative transfer calculations, as explained in the previous sections. Immediately after the cloud passed above our sensors, it entered the field of view of an accurate particle sizing device (Spraytec, Malvern, UK), which continuously measured the volume size distribution of the droplets.

As stated before, the purpose of the controlled experiment was to validate the proposed methodology. Unfortunately, the air-atomizing nozzle cannot produce a droplets size distribution which follows the Modified Gamma size distribution (Eq. 2). The differences between these size distributions are revealed in Fig. 21. Whereas the Modified Gamma size distribution is characterized by a distinct peak and absence of droplets below a certain threshold, the nozzle produces number concentration which is almost monotonic decreasing. Since one of the basic concepts in our method is spectral match between the measured differential signal and a spectral library created by a radiative transfer model, and since the predicted signal strongly depends on the droplets size distribution, it is essential the spectral library would be based on correct information regarding the droplets size distribution. Therefore, we have used droplets size distribution readings of the Spraytec during the experiment as an input for MODTRAN to create the spectral library. Figure 22 presents the cross SAM matrix of the differential signals which were created for the validation experiment. Comparing Fig. 22 and Fig. 8 reveals the differences between the validation experiment and the theoretical capabilities of the method regarding natural clouds. Two main distinct areas exist in the cross SAM matrix in Fig. 22: spray with effective radius of less than 4 µm differs from spray

AMTD
4, 7277–7335, 2011

with higher effective radius. The ability to distinguish between sprays within the two areas is quite small.

After the proper spectral library was created, we have utilized the proposed methodology. As described in Sect. 2.4, the rationale behind the retrieval methodology is to choose the possible solutions that match our observation and produce the best results in terms of both spectral fitness and signal magnitude. Specifically, the following scheme was used to determine the valid solution space for every measured spectrum:

A. Let I be a spectral signature of the zenith sky at some point in the analyzed time frame, and let S be the spectral library of the differential spectral signatures of the simulated clouds.

B. Let I_{ref} represent the clear sky spectrum (measured by the SR5000 just before the artificial cloud was sprayed).

C. We define the measured differential spectral signature to be $\Delta I = I - I_{ref}$.

D. Let SAM_{RES} be a vector containing the calculated SAM values between ΔI and every signature in S.

E. Let S_{sub} be a subset of S which contains all the differential spectral signatures of the simulated clouds, for whom the SAM_{RES} is smaller than 10°.

F. Let RMS_{sub} be a vector of the root-mean-square (RMS) value of the spectral difference between every signature in S_{sub} and ΔI.

G. Naturally, the simulated cloud with the lowest RMS value in RMS_{sub} corresponds to the best solution of the retrieval method. Nevertheless, and in order to allow a certain space of valid solutions, we consider the 10 simulated clouds which produced the lowest RMS values in the RMS_{sub} vector to be the valid solutions for the measured signal I.

AMTD
4, 7277–7335, 2011

Figure 23 presents the results of the validation experiment. The blue line is the effective radius of the artificial cloud as measured by the Spraytec, while the green line is the effective radius which was retrieved by the proposed method. One can notice that the retrieval largely agrees with the Spraytec's readings: if we define agreement between the Spraytec's and the retrieval's effective radii as a case where the Spraytec's effective radius does not deviate by more than 30 % of the retrieval effective radius range, then the Spraytec and the retrieval agree more than 70 % of the time. Some of the disagreements between the graphs are likely the result of the inevitable differences between the line of sights of the two optical devices: the Spraytec was positioned horizontally in a manner that assured most of the cloud entered its field of view all of the time. The SR5000, on the contrary, was pointed to the zenith with a mere field of view of 6 mrad which corresponds to approximately 100 mm^2 of the passing cloud. This setup made the retrieval of the SR5000 much more sensitive to wind fluctuations (Fig. 24).

5 Conclusions and discussion

A new concept for the retrieval of the microphysical and optical properties of very thin water clouds is proposed. The method utilizes ground based measurements which exploit high spectral, spatial, and temporal resolutions, and allow a study of cloud small scale dynamics and evolution, which cannot be measured in fine details from space, due to the sensor's insufficient temporal and spatial resolution. The retrieval methodology is composed of 3 elements: radiative transfer model, enhancement of the signal by subtraction of clear sky reference, and spectral matching method. The theoretical limitations of the methodology have been discussed, and the current estimate is a liquid water path range of 0.065–49.26 $\mathrm{g\,m^{-2}}$, and a lower limit of about 0.01 visible optical depth. These thin clouds are practically ignored in common remote sensing measurements of cloud's properties as well as global circulation models, although their frequency (and their total radiative forcing) is expected to be high. The

AMTD

4, 7277–7335, 2011

proposed methodology was validated in a controlled experiment where artificial clouds were sprayed and their effective radii were measured by an accurate particle sizing device and retrieved by the method simultaneously. We have also shown that changes in relative humidity, aerosols, and haze cannot be attributed as the source for the measured changes in the sky radiance, as their effects differ by either the expected spectral behaviour or the magnitude of the signal.

This methodology and ongoing measurements might prove useful in several aspects. First, it can be used to study the frequency and radiative forcing of thin water clouds, and, in addition, to study how they are influenced by anthropogenic activity (e.g. whether the aerosol loading in the atmosphere alters thin clouds properties). Second, this method can be used to study the cloud's "twilight zone", as comparison to standard optical depth measurements (either from space-borne platforms such as MODIS or from ground based instruments such as the AERONET) can be easily achieved. Third, it is possible to study the microphysical processes which control cloud's edges, as this method can retrieve their spatial and temporal characteristics. Finally, this method can be further expanded to study what seems as optically clear sky conditions, in a search for unique phenomena that could be spectrally analyzed.

A field campaign was conducted during the summers of 2010 and 2011, and the optical and microphysical properties of thin clouds were retrieved by the proposed method. The results of this campaign will be published in a following paper.

Acknowledgements. The authors are thankful to Amnon Sharon and Nadav Gilad for their essential technical support in conducting the validation experiment. This research was partly funded by the Israeli Ministry of Science and Technology (IMOS – Tashtiot) grant.

References

"Aerosol Robotic Network (AERONET) Homepage": http://aeronet.gsfc.nasa.gov/, December, 2010.

"Atmospheric Sounding": available at: http://weather.uwyo.edu/upperair/sounding.html, May, 2011.

Agassi, E., Ronen, A., Shiloah, N., and Hirsch, E.: Discrimination between natural dense dust clouds with IR spectral measurements, International Journal of High Speed Electronics and Systems, 18, 647–660, 2008.
Berk, A., Bernstein, L. S., and Robertson, D. C.: MODTRAN: A moderate resolution model for LOWTRAN 7, Tech. Rep. GLTR-89-0122, Geophysics Laboratory, Air Force System Command, Hanscom AFB, Massachusetts, 1989.
Deirmendjian, D.: Scattering and Polarization Properties of Water Clouds and Hazes in the Visible and Infrared, Appl. Optics, 3, 187–196, 1964.
Frisch, S., Shupe, M., Djalalova, I., Feingold, G., and Poellot, M.: The Retrieval of Stratus Cloud Droplet Effective Radius with Cloud Radars, J. Atmos. Ocean. Tech., 19, 835–842, doi:10.1175/1520-0426(2002)019<0835:TROSCD>2.0.CO;2, 2002.
Han, Y. and Westwater, E. R.: Remote Sensing of Tropospheric Water Vapor and Cloud Liquid Water by Integrated Ground-Based Sensors, J. Atmos. Ocean. Tech., 12, 1050–1059, doi:10.1175/1520-0426(1995)012<1050:RSOTWV>2.0.CO;2, 1995.
Hansen, J. E. and Travis, L. D.: Light scattering in planetary atmospheres, Space Sci. Rev., 16, 527–610, doi:10.1007/bf00168069, 1974.
Heintzenberg, J. and Charlson, R. J. (Eds.): Clouds in the perturbed climate system; their relationship to energy balance, atmospheric dynamics, and precipitation, The MIT Press, Cambridge, Massachusetts, 2009.
Hirsch, E. and Agassi, E.: Detection of gaseous plumes in IR hyperspectral images using hierarchical clustering, Appl. Optics, 46, 6368–6374, 2007.
Holben, B. N., Eck, T. F., Slutsker, I., Tanré, D., Buis, J. P., Setzer, A., Vermote, E., Reagan, J. A., Kaufman, Y. J., Nakajima, T., Lavenu, F., Jankowiak, I., and Smirnov, A.: AERONET-A Federated Instrument Network and Data Archive for Aerosol Characterization, Remote Sens. Environ., 66, 1–16, doi:10.1016/s0034-4257(98)00031-5, 1998.
IPCC: Climate Change 2007: The Physical Science Basis. Contribution of Working Group I to the Fourth Assessment Report of the Intergovernmental Panel on Climate Change , edited by: Solomon, S., Qin, D., Manning, M., Chen, Z., Marquis, M., Averyt, K. B., Tignor, M., and Miller, H. L., Cambridge University Press, Cambridge, United Kingdom and New York, NY, USA, 995 pp., 2007.
Johnson, R. A. and Wichern, D. W.: Applied multivariate statistical analysis, Third edition, Prentice-Hall International Inc., USA, 1992.
King, M. D., Tsay, S.-C., Platnick, S. E., Wang, M., and Liou, K.-N.: Cloud retrieval algorithms

for MODIS: optical thickness, effective particle radius, and thermodynamic phase, MODIS Algorithm Theoretical Basis Document, No. ATBD-MOD-05, MOD06 – Cloud product, 1997.

King, M. D., Platnick, S., Yang, P., Arnold, G. T., Gray, M. A., Riedi, J. C., Ackerman, S. A., and Liou, K.-N.: Remote Sensing of Liquid Water and Ice Cloud Optical Thickness and Effective Radius in the Arctic: Application of Airborne Multispectral MAS Data, J. Atmos. Ocean. Tech., 21, 857–875, doi:10.1175/1520-0426(2004)021<0857:RSOLWA>2.0.CO;2, 2004.

Kohler, H.: The nucleus in and the growth of hygroscopic droplets, Transactions of the Faraday Society, 32, 1152–1161, 1936.

Koren, I., Remer, L. A., Kaufman, Y. J., Rudich, Y., and Martins, J. V.: On the twilight zone between clouds and aerosols, Geophys. Res. Lett., 34, L08805, doi:10.1029/2007gl029253, 2007.

Koren, I., Oreopoulos, L., Feingold, G., Remer, L. A., and Altaratz, O.: How small is a small cloud?, Atmos. Chem. Phys., 8, 3855–3864, doi:10.5194/acp-8-3855-2008, 2008.

Koren, I., Remer, L. A., Altaratz, O., Martins, J. V., and Davidi, A.: Aerosol-induced changes of convective cloud anvils produce strong climate warming, Atmos. Chem. Phys., 10, 5001–5010, doi:10.5194/acp-10-5001-2010, 2010.

Kruse, F. A., Lefkoff, A. B., Boardman, J. W., Heidebrecht, K. B., Shapiro, A. T., Barloon, P. J., and Goetz, A. F. H.: The spectral image-processing system (SIPS) – interactive visualization and analysis of imaging spectrometer data, Remote Sens. Environ., 44, 145–163, 1993.

Markowicz, K. M., Flatau, P. J., Vogelmann, A. M., Quinn, P. K., and Welton, E. J.: Clear-sky infrared aerosol radiative forcing at the surface and the top of the atmosphere, Q. J. Roy. Meteor. Soc., 129, 2927–2947, doi:10.1256/qj.02.224, 2003.

Mätzler, C.: MATLAB Functions for Mie scattering and absorption, IAP Res. Rep. No. 02–08 (Institut für Angewandte, 2002).

McCaa, D. J. and Shaw, J. H.: The infrared spectrum of ozone, J. Mol. Spectrosc., 25, 374–397, doi:10.1016/s0022-2852(68)80050-5, 1968.

Mie, G.: Beiträge zur Optik trüber Medien, speziell kolloidaler Metallösungen, Ann. Phys., 330, 377–445, doi:10.1002/andp.19083300302, 1908.

Miles, N. L., Verlinde, J., and Clothiaux, E. E.: Cloud Droplet Size Distributions in Low-Level Stratiform Clouds, J. Atmos. Sci., 57, 295–311, doi:10.1175/1520-0469(2000)057<0295:cdsdil>2.0.co;2, 2000.

Nakajima, T. and King, M. D.: Determination of the Optical Thickness and Effective Particle Radius of Clouds from Reflected Solar Radiation Measurements. Part

I: Theory, Journal of the Atmospheric Sciences, 47, 1878–1893, doi:10.1175/1520-0469(1990)047<1878:DOTOTA>2.0.CO;2, 1990.

Nilsson, B.: Meteorological influence on aerosol extinction in the 0.2–40-µm wavelength range, Appl. Optics, 18, 3457–3473, 1979.

Palik, E.: Handbook of Optical Constants of Solids (5 Volume Set), {Academic Press}, 1997.

Park, B., Windham, W. R., Lawrence, K. C., and Smith, D. P.: Contaminant Classification of Poultry Hyperspectral Imagery using a Spectral Angle Mapper Algorithm, Biosystems Engineering, 96, 323–333, doi:10.1016/j.biosystemseng.2006.11.012, 2007.

Ramanathan, V., Cess, R. D., Harrison, E. F., Minnis, P., Barkstrom, B. R., Ahmad, E., and Hartmann, D.: Cloud-Radiative Forcing and Climate: Results from the Earth Radiation Budget Experiment, Science, 243, 57–63, doi:10.1126/science.243.4887.57, 1989.

Richwine, L. J., Clapp, M. L., Miller, R. E., and Worsnop, D. R.: Complex refractive indices in the infrared of nitric acid trihydrate aerosols, Geophys. Res. Lett., 22, 2625–2628, doi:10.1029/95gl02650, 1995.

Rodgers, C. D.: Inverse Methods for Atmospheric Sounding: Theory and Practice, edited by: Taylor, F. W., Oceanic and Planetary Physics, World Scientific, 2, 2000.

Rothman, L. S., Barbe, A., Benner, D. C., Brown, L. R., Camy-Peyret, C., Carleer, M. R., Chance, K., Clerbaux, C., Dana, V., Devi, V. M., Fayt, A., Flaud, J. M., Gamache, R. R., Goldman, A., Jacquemart, D., Jucks, K. W., Lafferty, W. J., Mandin, J. Y., Massie, S. T., Nemtchinov, V., Newnham, D. A., Perrin, A., Rinsland, C. P., Schroeder, J., Smith, K. M., Smith, M. A. H., Tang, K., Toth, R. A., Vander Auwera, J., Varanasi, P., and Yoshino, K.: The HITRAN molecular spectroscopic database: edition of 2000 including updates through 2001, J. Quant. Spectrosc. Ra. , 82, 5–44, 2003.

Slingo, A.: Sensitivity of the Earth's radiation budget to changes in low clouds, Nature, 343, 49–51, 1990.

"Station Observations": available at: http://weather.uwyo.edu/surface/meteogram/, August, 2010.

Stephens, G. L.: Remote Sensing of the Lower Atmosphere. An Introduction, Oxford University Press, 523 pp., 1994.

Thomas, G. E., Bass, S. F., Grainger, R. G., and Lambert, A.: Retrieval of aerosol refractive index from extinction spectra with a damped harmonic-oscillator band model, Appl. Optics, 44, 1332–1341, 2005.

Toon, O. B., Pollack, J. B., and Khare, B. N.: The optical constants of several atmospheric aerosol species: ammonium sulfate, aluminum oxide, and sodium chloride, J. Geophys. Res., 81, 5733–5748, 1976.

Trenberth, K. E., Fasullo, J. T., and Kiehl, J.: Earth's Global Energy Budget, B. Am. Meteorol. Soc., 90, 311–323, doi:10.1175/2008bams2634.1, 2009.

Tselioudis, G. and Jakob, C.: Evaluation of midlatitude cloud properties in a weather and a climate model: Dependence on dynamic regime and spatial resolution, J. Geophys. Res., 107, 4781, doi:10.1029/2002jd002259, 2002.

Turner, D. D.: Arctic Mixed-Phase Cloud Properties from AERI Lidar Observations: Algorithm and Results from SHEBA, J. Appl. Meteorol., 44, 427–444, doi:10.1175/JAM2208.1, 2005.

Turner, D. D., Vogelmann, A. M., Austin, R. T., Barnard, J. C., Cady-Pereira, K., Chiu, C., Clough, S. A., Flynn, C. J., Khaiyer, M. M., Liljegren, J. C., Johnson, K. L., Lin, B., Long, C. N., Marshak, A., Matrosov, S. Y., McFarlane, S. A., Miller, M. A., Min, Q., Minnis, P., O'Hirok, W., Wang, Z., and Wiscombe, W. J.: Thin Liquid Water Clouds: Their Importance and Our Challenge, B. Am. Meteorol. Soc., 88, 177–190, 2007.

Volz, F. E.: Infrared Refractive Index of Atmospheric Aerosol Substances, Appl. Optics, 11, 755–759, 1972.

Volz, F. E.: Infrared Optical Constants of Ammonium Sulfate, Sahara Dust, Volcanic Pumice, and Flyash, Appl. Optics, 12, 564–568, 1973.

Weng, F., and Grody, N. C.: Retrieval of cloud liquid water using the special sensor microwave imager (SSM/I), J. Geophys. Res., 99, 25535–25551, doi:10.1029/94jd02304, 1994.

Wylie, D., Jackson, D. L., Menzel, W. P., and Bates, J. J.: Trends in Global Cloud Cover in Two Decades of HIRS Observations, J. Climate, 18, 3021–3031, doi:10.1175/JCLI3461.1, 2005.

Yamamoto, G., Tanaka, M., and Asano, S.: Radiative Transfer in Water Clouds in the Infrared Region, J. Atmos. Sci., 27, 282–292, http://dx.doi.org/10.1175/1520-0469(1970)027¡0282:RTIWCI¿2.0.CO;2doi:10.1175/1520-0469(1970)027<0282:RTIWCI>2.0.CO;2, 1970.

Yuhas, R. H., Goetz, A. F. H., and Boardman, J. W.: Discrimination among semi-arid landscape endmembres using the spectral angle mapper (SAM) algorithm, in: Summaries of the 3rd annual JPL Airborne Geoscience Workshop, Jet Propulsion Laboratory, Pasadena, CA, 147–149, 1992.

Table 1. Parameters of clouds droplet size distributions used in our simulation (right column), and as summarized from vast in-situ measurements of droplets size distributions in low-level continental and marine Stratiform clouds (Miles et al., 2000). Values in parenthesis represent the parameter's standard deviation.

Parameter	In-situ measurements (Miles et al., 2000)		Simulated droplets size distributions
	Continental	Marine	
Mean radius [µm]	4.1 (1.95)	7.1 (1.7)	6.3 (3.8)
Standard deviation above mean radius [µm]	1.55 (0.6)	2.9 (1)	3.4 (2.7)
Effective radius [µm]	5.4 (2.05)	9.6 (2.35)	9.6 (6.5)
LWC [$mg\,m^{-3}$]	190 (210)	180 (140)	118 (128)

AMTD
4, 7277–7335, 2011

Table 2. The range of the LWC, LWP, r_{eff}, thickness, and optical depths of the simulated clouds.

Liquid water content [$mg\,m^{-3}$]	Liquid water path [$g\,m^{-2}$]	Cloud's depth [m]	Effective radius [µm]	Optical Depth ($\lambda = 550\,nm$)	Optical Depth ($\lambda = 10\,\mu m$)
2.6–500	0.065–49.26	10–100	0.16–20	9.4×10^{-3}–138	8.5×10^{-3}–4.48

AMTD
4, 7277–7335, 2011

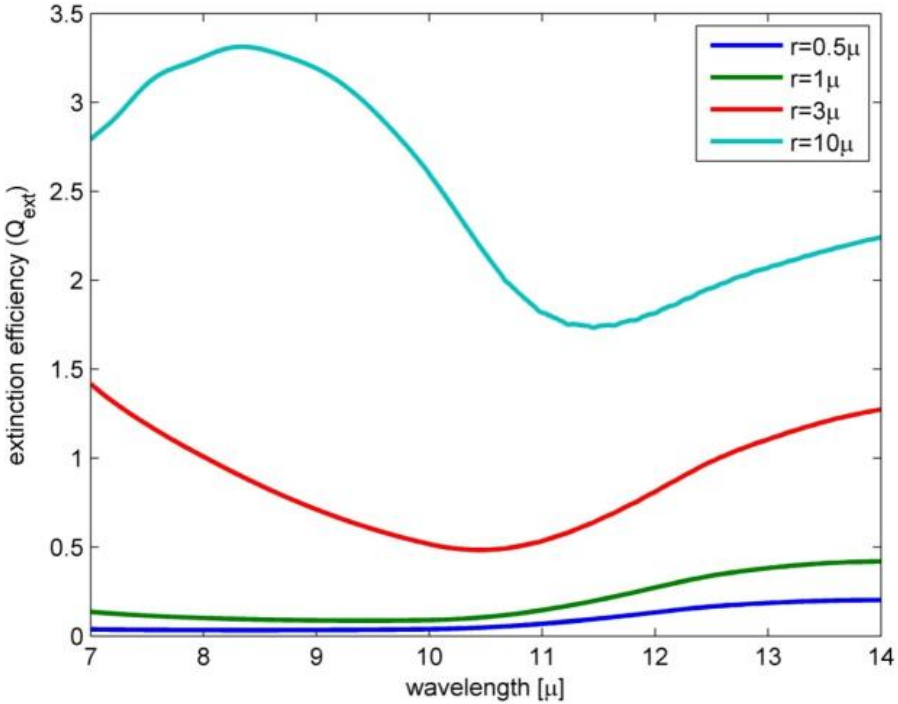

Fig. 1. Extinction efficiency vs. wavelength for water droplets at different radii. Note the evident spectral difference of the various droplets. This analysis suggests that thin water clouds which differ by their droplet's effective radius, might have a unique spectrum in the LWIR. As a result, it might be possible to discriminate between water droplets of different sizes.

AMTD
4, 7277–7335, 2011

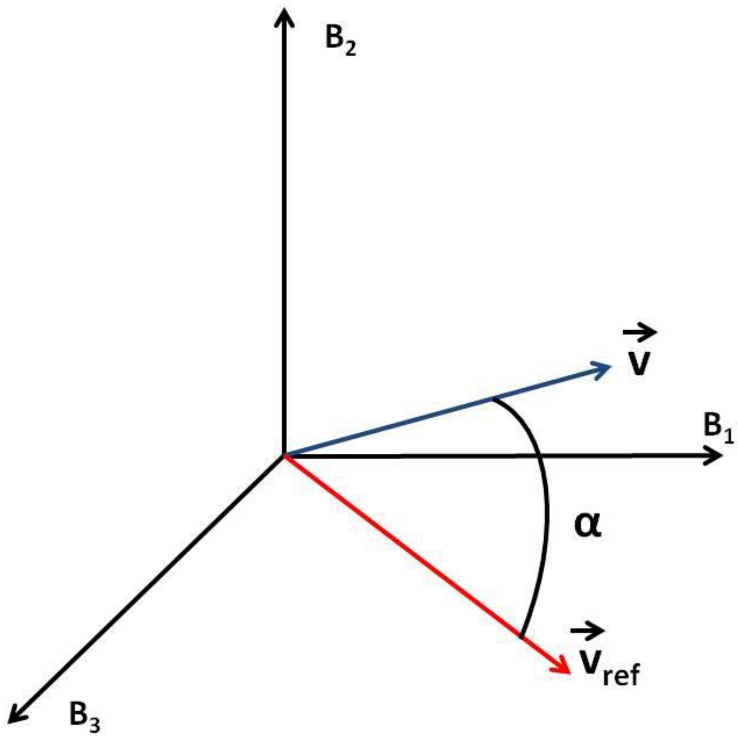

Fig. 2. An example of the SAM (Spectral Angle Mapping) index of two spectra. SAM considers a measured spectrum in n wavelengths ($n = 3$ in this example) as a vector in an n dimensional space (B_1, B_2, B_3). The spectral similarity between a measured spectrum ($\boldsymbol{V}$) and a reference spectrum ($\boldsymbol{V}_{\mathrm{ref}}$) is simply the angle α between these two spectra, calculated to be $\alpha = \cos^{-1}$ $\left(\frac{\boldsymbol{V}\cdot\boldsymbol{V}_{\mathrm{ref}}}{\|\boldsymbol{V}\|\cdot\|\boldsymbol{V}_{\mathrm{ref}}\|}\right)$. Distinct spectra will produce relatively large SAM values, while similar spectra will produce small values.

AMTD
4, 7277–7335, 2011

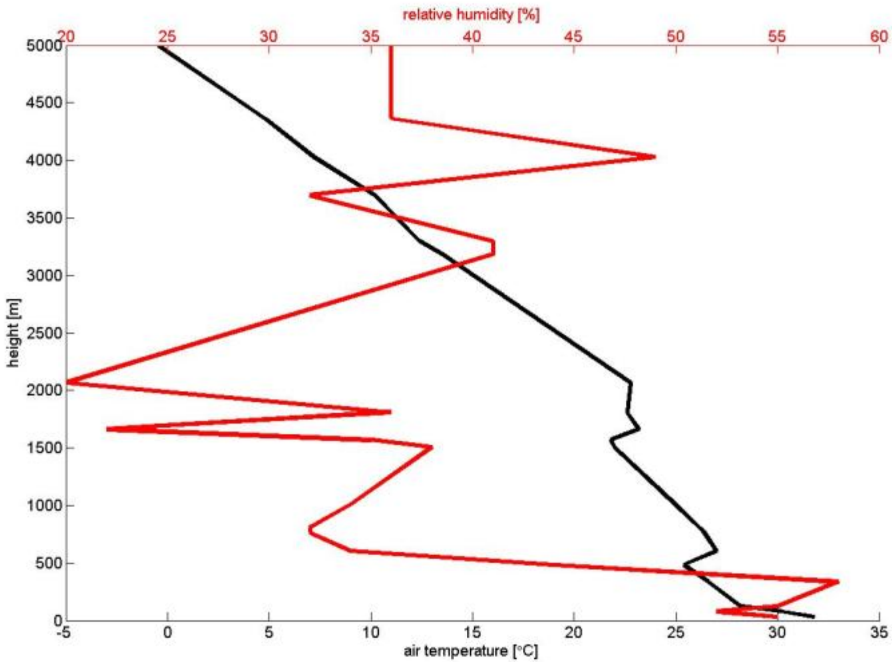

Fig. 3. Atmospheric profile (relative humidity in red, and air temperature in black) on 8 August 2010, 12:00 UTC (Website: "Atmospheric Sounding"). The shallow inversion layer is noticeable at a height of about 600 m.

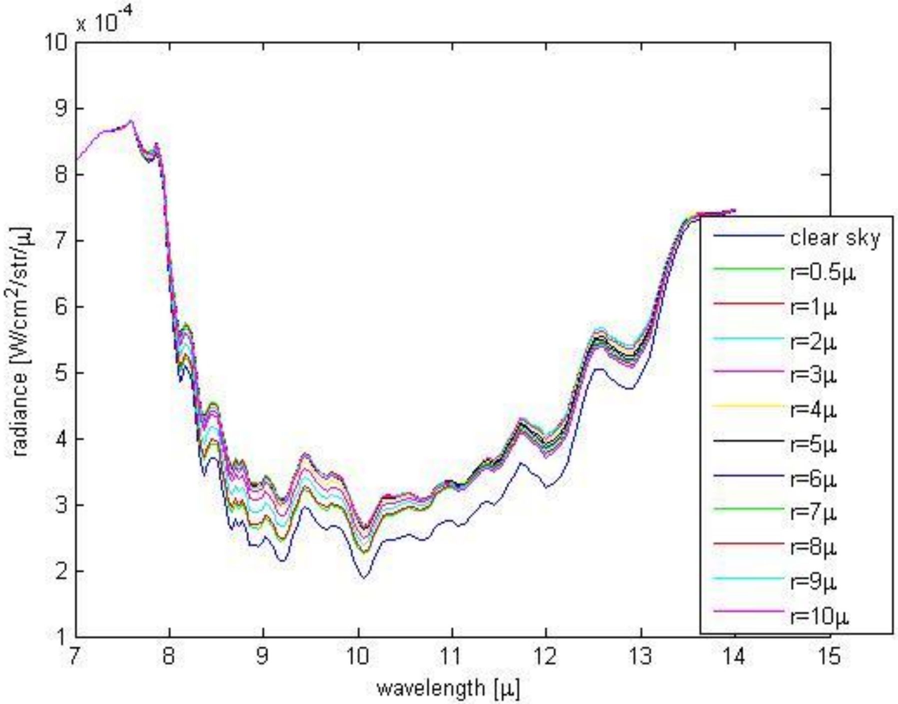

Fig. 4. The expected spectral signature of the zenith sky in the presence of 50 m thick monodisperse clouds with liquid water content of 15 mg m^{-3} at 800 m above the ground. Every cloud is characterized by different water droplets radii. At first glance, the spectral signatures appear extremely similar.

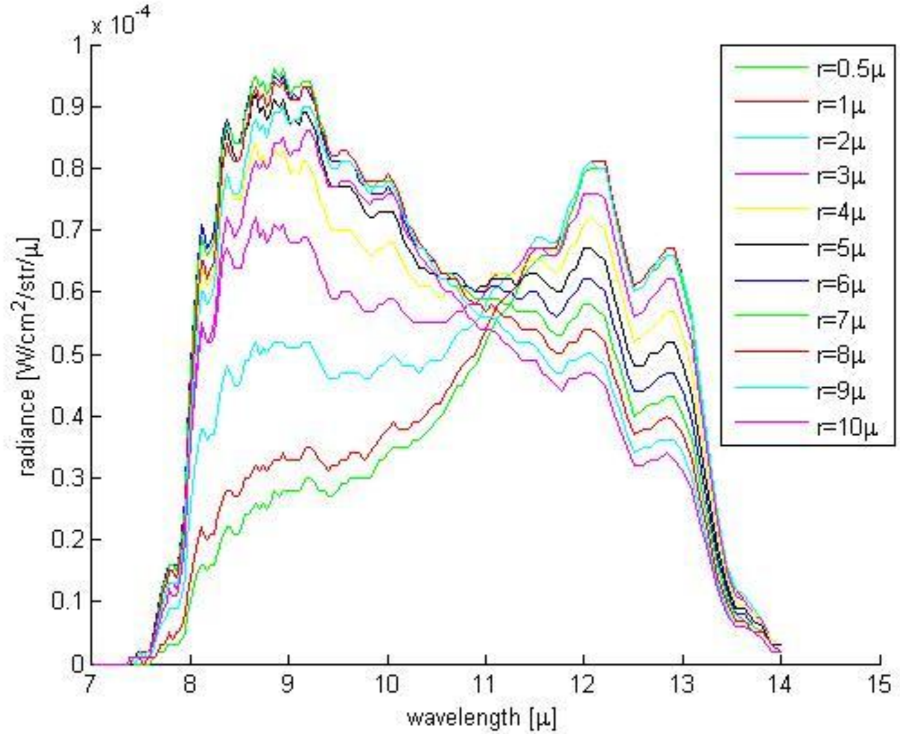

Fig. 5. The differential spectral signature of the various clouds presented in Fig. 4. Every signature in this figure is the result of subtracting the clear sky signature (see Fig. 4) from the expected sky radiance in the presence of a cloud. One can notice the evident spectral difference caused by different water droplets' radii. Clouds with small water droplets attenuate more radiation in the 11 µm–13 µm, while clouds with larger droplets affect more in the 8 µm–9 µm.

AMTD
4, 7277–7335, 2011

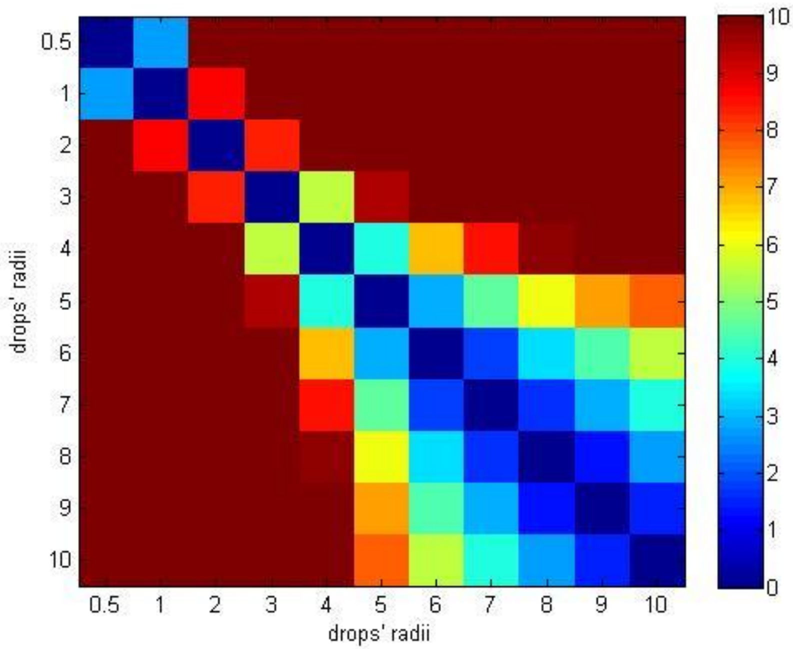

Fig. 6. Cross SAM values of the differential spectral signatures formed by thin clouds (Fig. 5). Small values indicate the signatures are spectrally similar, while large values indicate the signatures are spectrally distinct. Three distinctive areas exist in the matrix: (1) small water droplets with radii less than 2 µm create spectral signatures which are relatively similar (low cross SAM values), while their spectral signature is distinctive from water droplets with higher radii. (2) Medium water droplets with radii of 2 µm–3 µm are unique from water droplets with other radii. (3) Spectral signatures of larger water droplets with radii higher than 4 µm appear spectrally different than smaller droplets, but the method's capability to distinguish between droplets in the region of 4 µm–10 µm is relatively low.

AMTD
4, 7277–7335, 2011

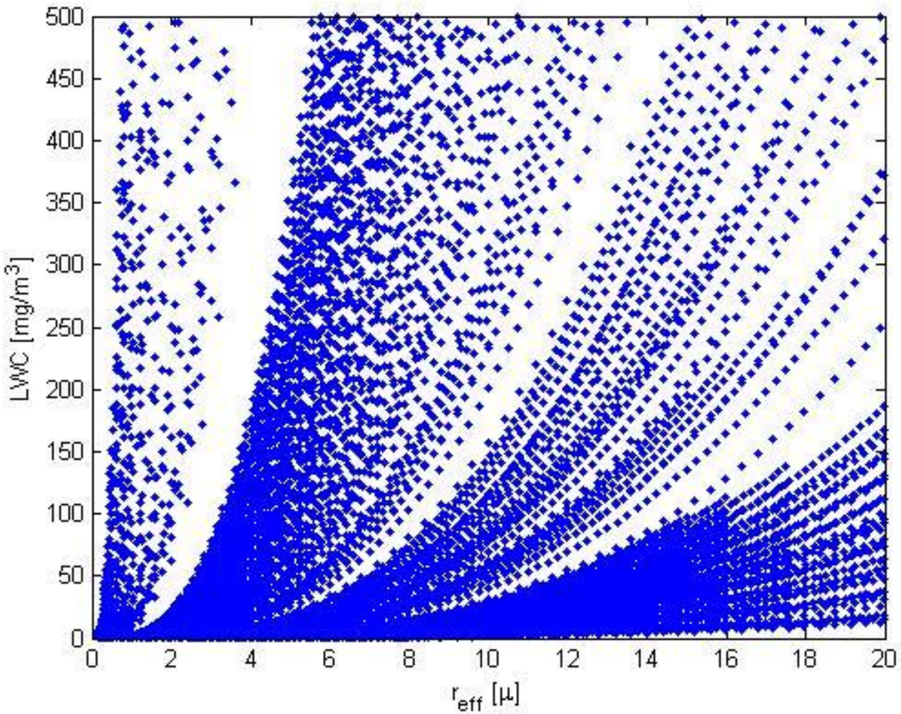

Fig. 7. The space of LWC and effective radius of the different clouds that were used in this analysis. Every point in this graph represents a modified Gamma size distribution with distinct parameters. The size distribution is used to calculate the extinction, absorption, and scattering coefficients for unit length of the simulated cloud.

AMTD
4, 7277–7335, 2011

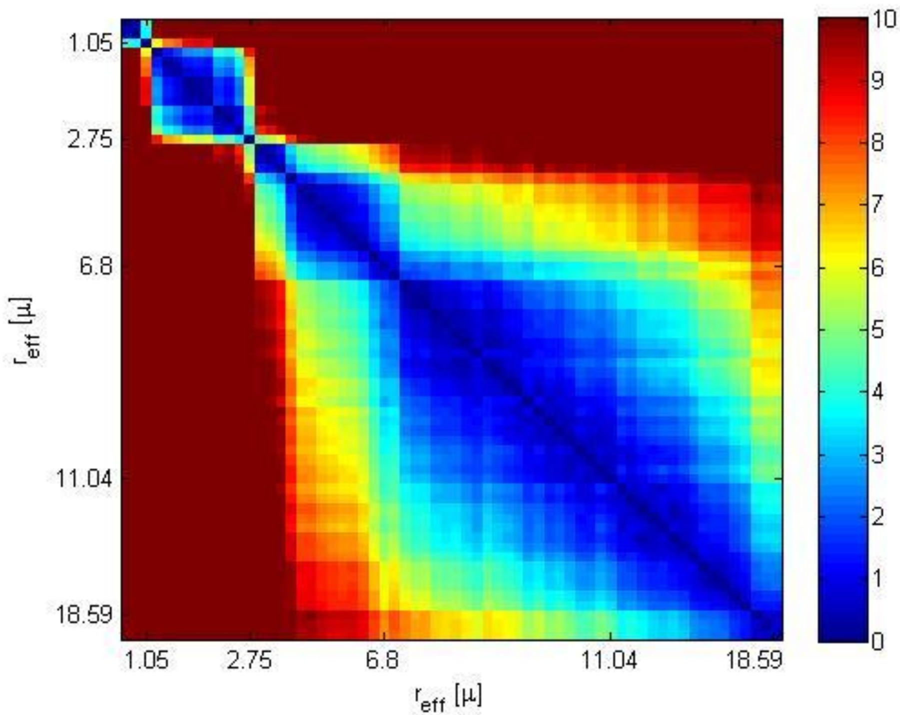

Fig. 8. Cross SAM values of the differential spectral signatures of water clouds with different effective radii with approximately constant LWC ($14.5\,\mathrm{mg\,m^{-3}} < \mathrm{LWC} < 15\,\mathrm{mg\,m^{-3}}$). This figure shows that the spectral variability depends on the effective radius of the cloud: clouds with small r_{eff} (less than 1 µm) are spectrally distinct, as their cross SAM values with other clouds are relatively high. Clouds with medium effective radius ($1\,\mu\mathrm{m} < r_{\mathrm{eff}} < 2.75\,\mu\mathrm{m}$) are easily distinguished by the SAM analysis. Clouds with $r_{\mathrm{eff}} > 3$ appear relatively similar to each other, but quite different from a cloud with smaller r_{eff}.

AMTD
4, 7277–7335, 2011

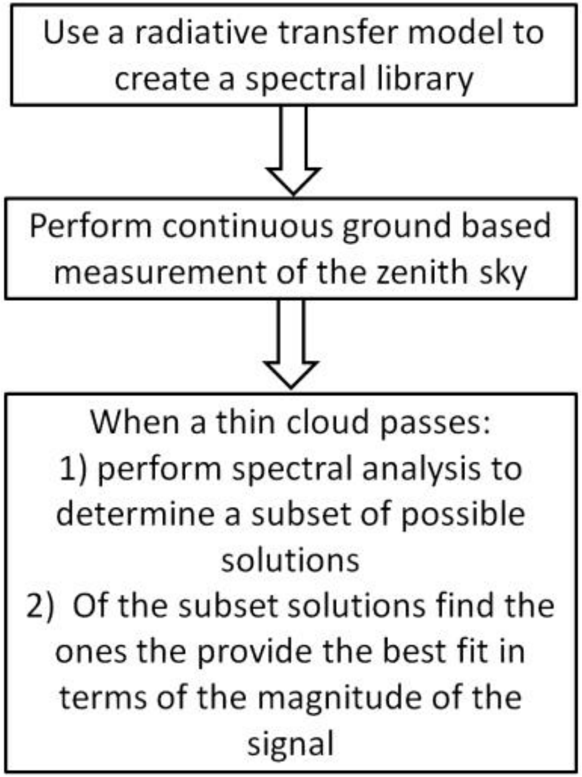

Fig. 9. A flowchart of the proposed methodology for the retrieval of very thin liquid water clouds' microphysical and optical properties.

AMTD
4, 7277–7335, 2011

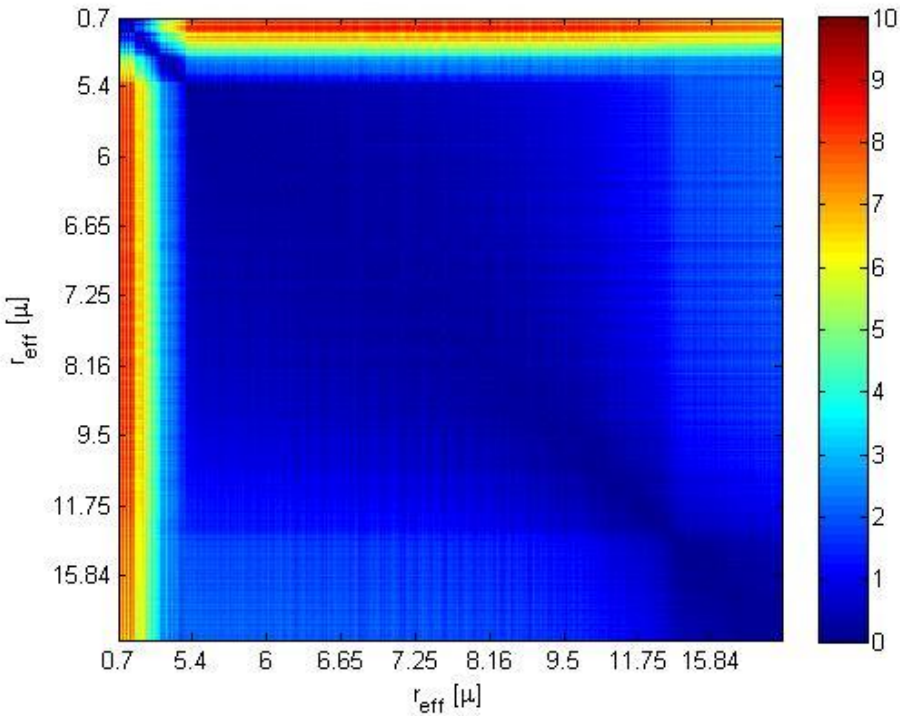

Fig. 10. Cross SAM values of the differential spectral signatures of water clouds with different effective radii with relatively high LWC of 400 mg m^{-3}–500 mg m^{-3}. Comparing this figure to Fig. 8, we see that the ability to spectrally distinguish clouds with different effective radius has worsened, as a result of the higher LWC values which cause the clouds' spectral signatures to approach the radiation spectrum emitted by a blackbody.

AMTD
4, 7277–7335, 2011

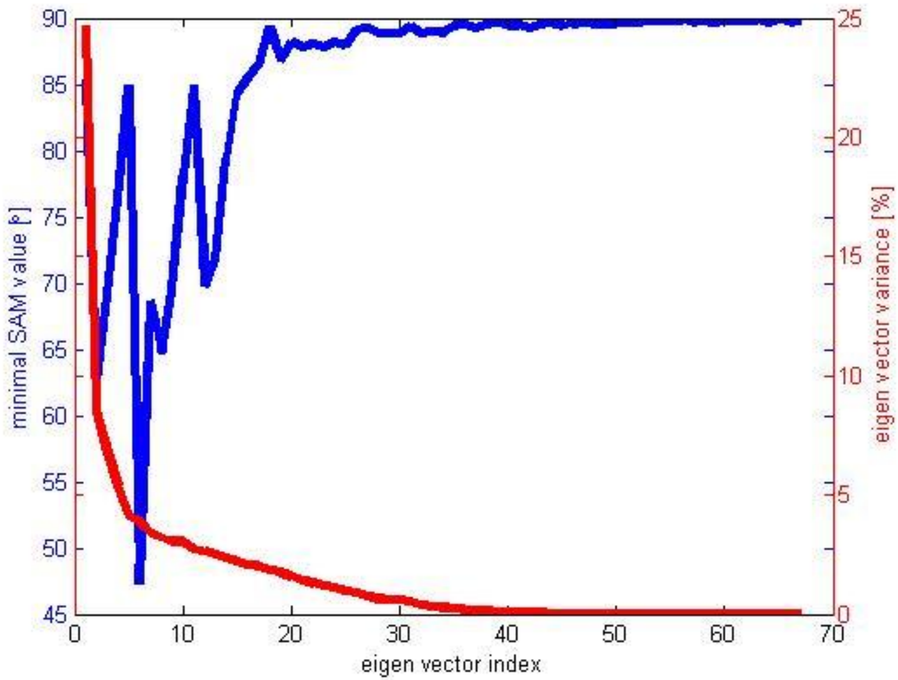

Fig. 11. The possible effect of inherent spectral noise of the measuring device on the proposed methodology. The eigenvectors are sorted according to their variance (red line), as commonly presented in principle component analysis. The blue line is the smallest (spectrally closest) SAM value between every eigenvector and the clouds spectral library. These high SAM values indicate that the inherent features spectrally differ from expected clouds signals, and cannot induce any misclassification on the proposed methodology.

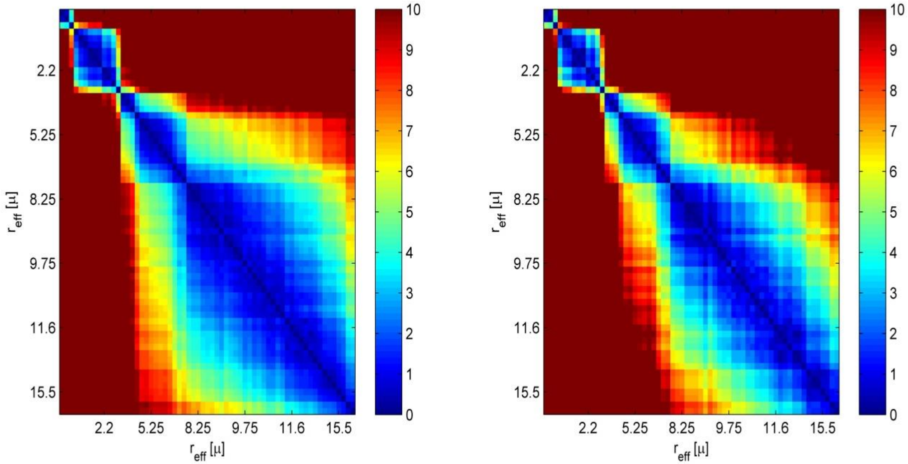

Fig. 12. The cross SAM matrix of differential spectral signals (of thin water clouds), using 67 spectral bands (left) and 5 spectral bands (right). One can notice the cross SAM matrix look similar which suggests that reduced number of bands can be used for the retrieval.

AMTD
4, 7277–7335, 2011

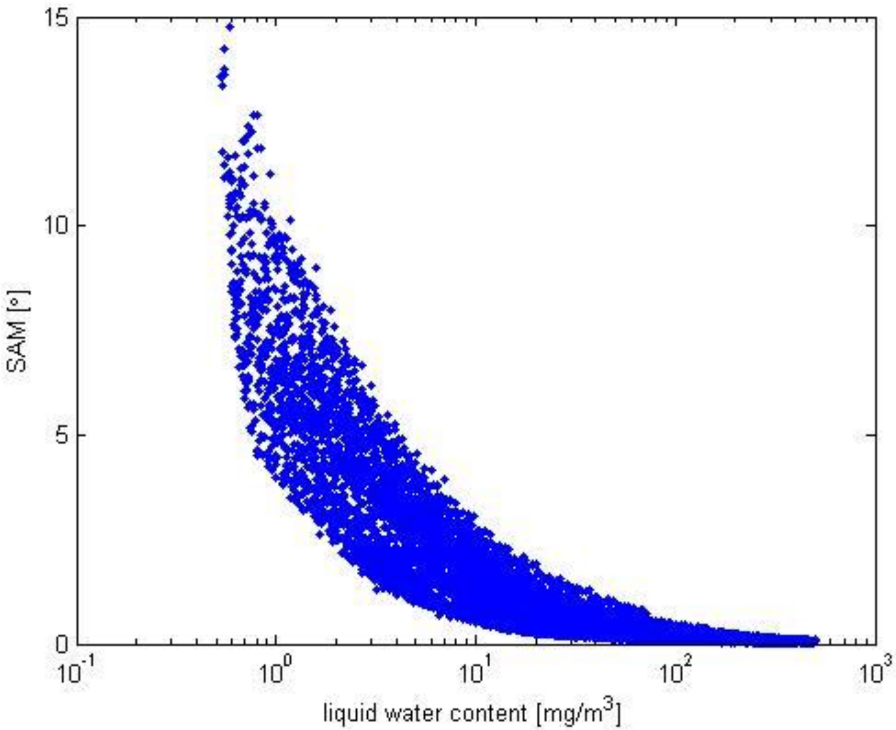

Fig. 13. SAM between every simulated cloud's differential spectral signature and the modified differential spectral signature which is the result of a 50 m thick layer (750 m–800 m) below the cloud, with the relative humidity as set to 50 %. The horizontal scale is the LWC of the simulated clouds. It is noticeable that only clouds with LWC less than 4 $mg\,m^{-3}$ might experience a spectral shift of more than 5° in the SAM index.

AMTD
4, 7277–7335, 2011

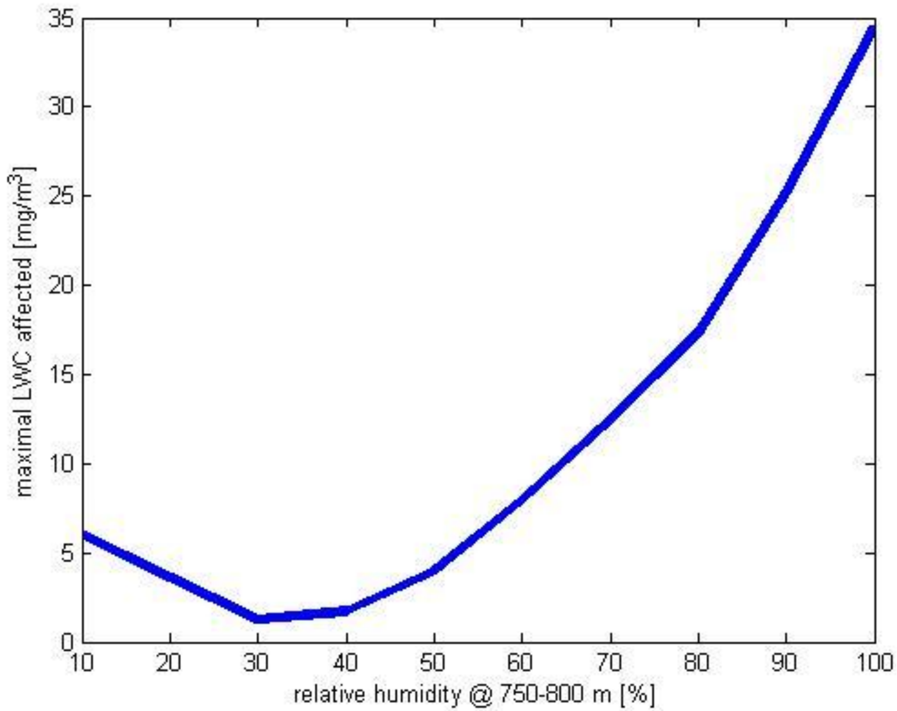

Fig. 14. Clouds with LWC lower than the values shown in the graph will be affected by variations in the relative humidity values of the layer below the clouds (750 m–800 m). A cloud is considered to be affected if its differential spectral signature differs by more the 5° (in terms of SAM) from the differential spectral signature of the modified cloud.

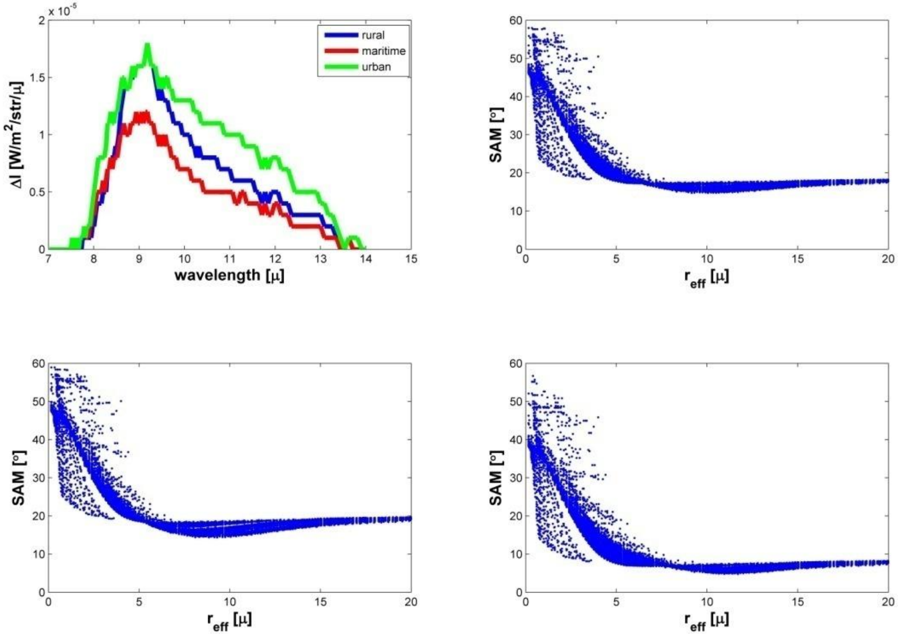

Fig. 15. Top left: the effect of atmospheric aerosols on the zenith sky spectrum. The differential spectrum of the zenith sky in the presence of an optically thick (AOT = 0.26), 50 m aerosol layer at 800–850 m. Top right: scatter plot of the SAM angle between the differential spectrum of rural aerosols and the differential spectrum of thin water clouds with a certain effective radius (x-axis). Bottom left: the same, but for maritime aerosols. Bottom right: the same, but for urban aerosols. It seems that rural and maritime aerosols do not show any spectral similarity, as the lowest SAM values are 14.76° and 14.35°, respectively. However, the urban aerosols effect appears similar to water clouds to some extent (minimal SAM angle of 4.79°), but the magnitude of the expected change is relatively small, even in the extreme simulated theoretical conditions.

AMTD

4, 7277–7335, 2011

Title Page
Abstract | Introduction
Conclusions | References
Tables | Figures
◀| |▶
◀ ▶
Back | Close
Full Screen / Esc
Printer-friendly Version
Interactive Discussion

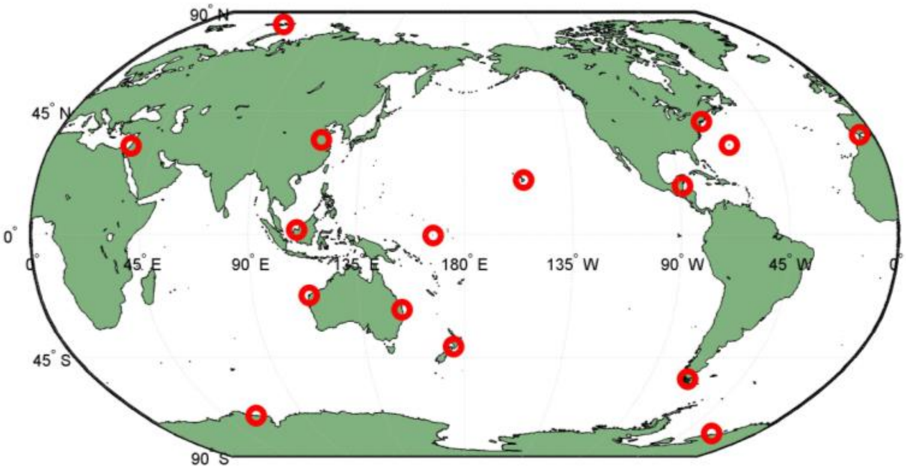

Fig. 16. The location of 16 worldwide meteorological stations (Website: "Atmospheric Sounding"), which were manually chosen. The atmospheric profile was measured simultaneously on 8 August 2010, 12:00 UTC. These locations represent wide range of seasonal, diurnal, and meteorological conditions (from Arctic across the tropics to Antarctica, and both summer and winter).

AMTD
4, 7277–7335, 2011

Optical and microphysical properties of thin warm clouds

E. Hirsch et al.

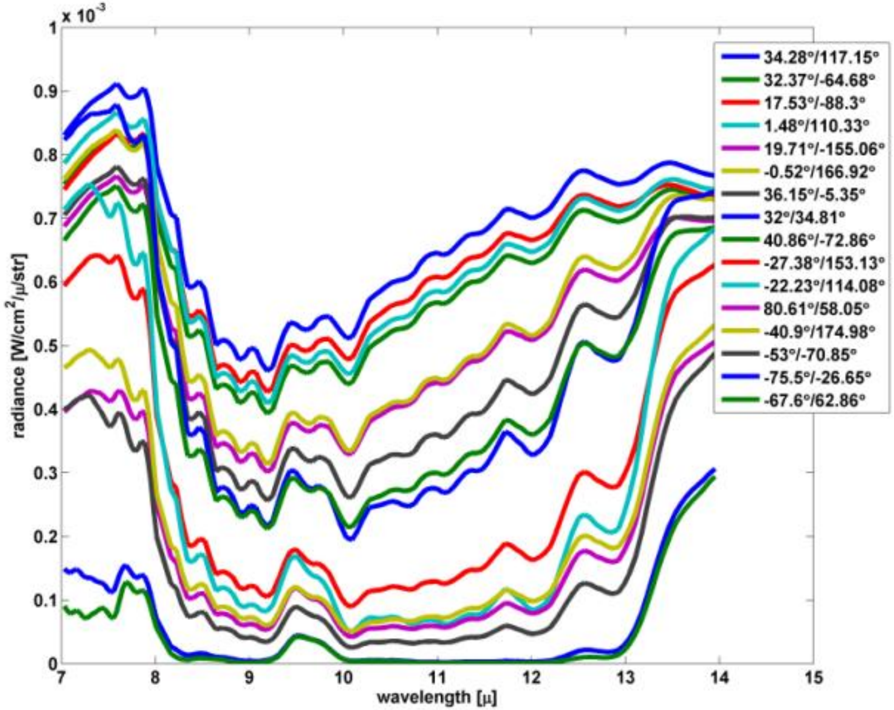

Fig. 17. The expected spectral radiance of the zenith clear sky under different atmospheric profiles.

AMTD
4, 7277–7335, 2011

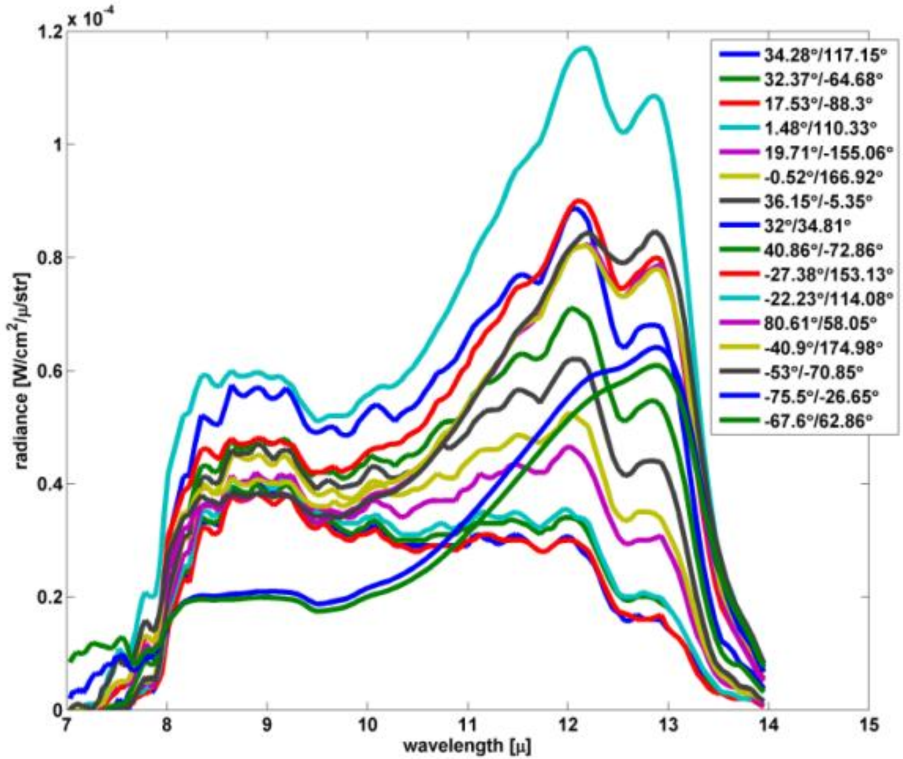

Fig. 18. The expected differential spectrum of a thin cloud under different atmospheric profiles. The cloud is characterized by and effective radius of 2.1 μm and LWP of 750 mg m^{-2}.

AMTD
4, 7277–7335, 2011

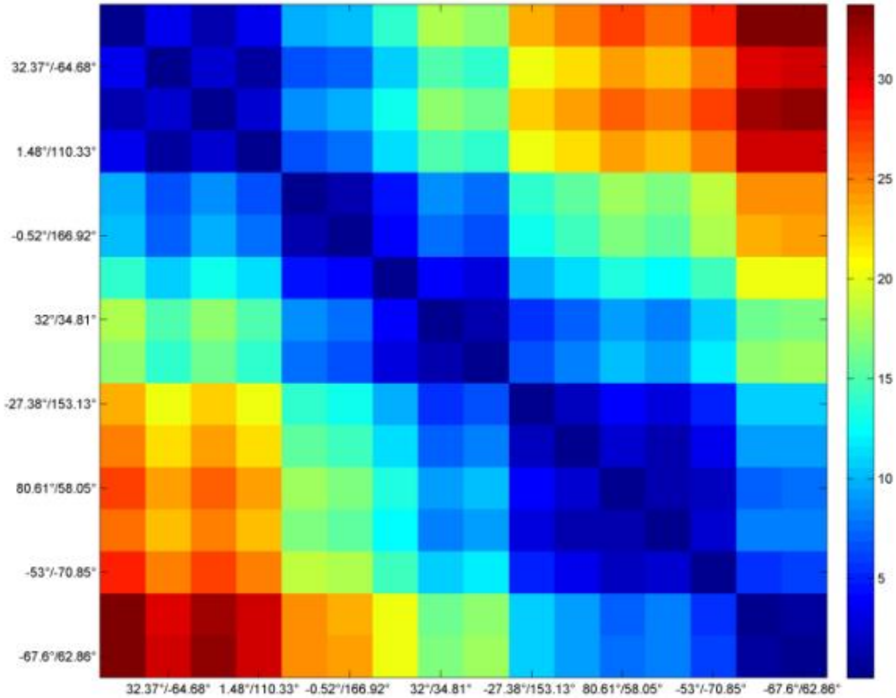

Fig. 19. Cross SAM values of differential spectrum of the same cloud under different atmospheric profiles. The axes labels indicate the latitude/longitude of the different meteorological stations.

AMTD
4, 7277–7335, 2011

Fig. 20. A controlled experimental setup for validation of the proposed methodology. An artificial cloud was sprayed via an air-atomizing nozzle and entered the field of view of an accurate particle sizing device (Spraytec). A calibrated spectro-radiometer and a thermal imager were positioned below the passing cloud (not shown), pointing to the zenith.

AMTD
4, 7277–7335, 2011

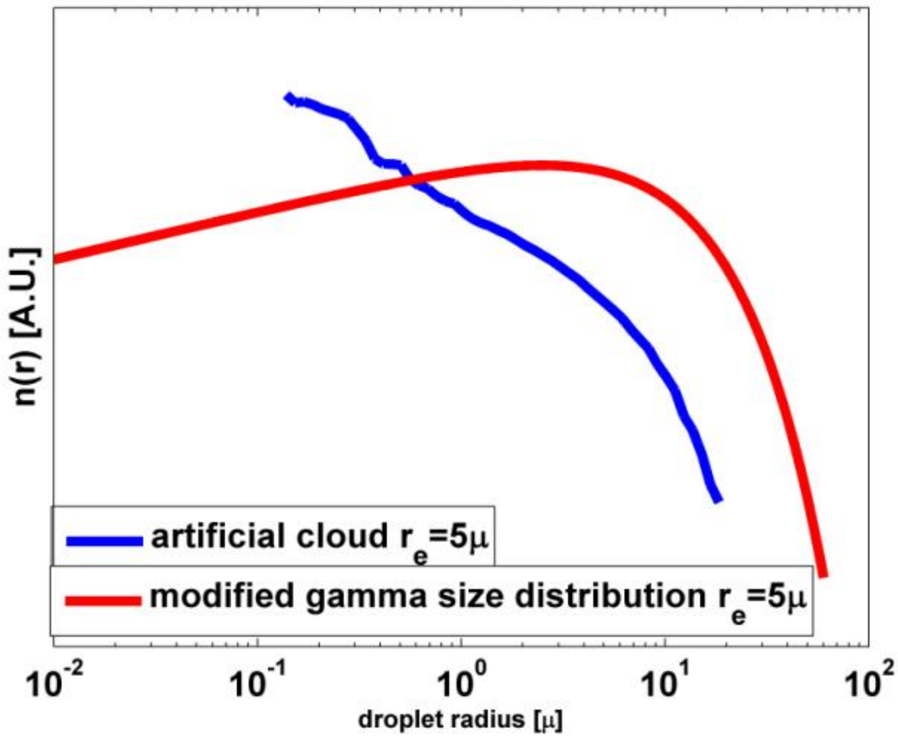

Fig. 21. Modified Gamma number size distribution (red), and the number size distribution produced by the air atomizing nozzle (blue). Both distributions are characterized by effective radius of 5 μm.

AMTD
4, 7277–7335, 2011

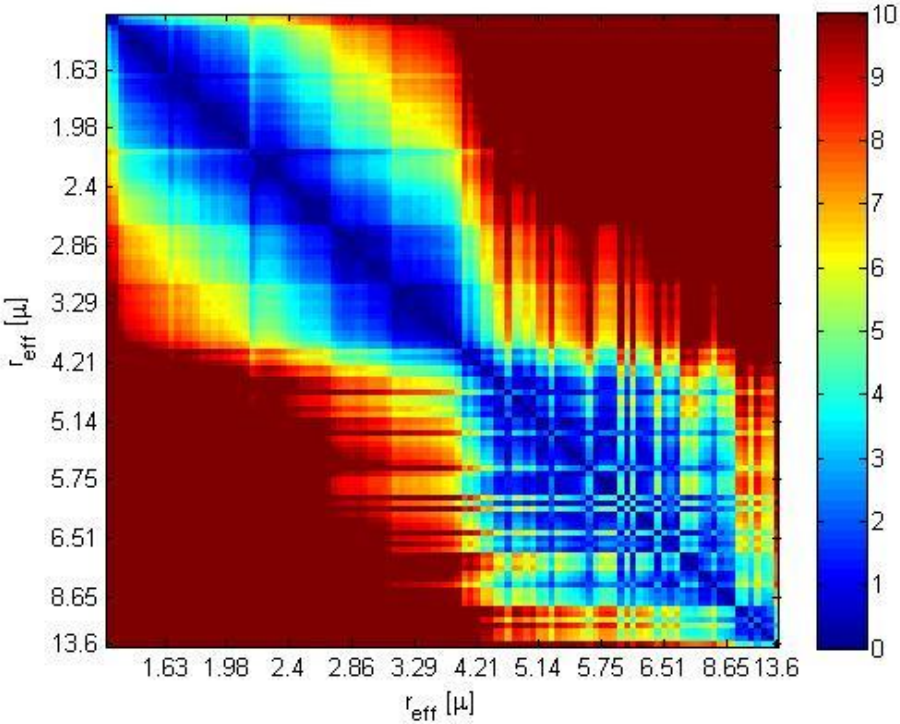

Fig. 22. Cross SAM matrix of differential signals of thin water cloud (LWC ~15 mg m^{-3}) that follow the droplets size distribution that is produced by the air-atomizing nozzle.

AMTD
4, 7277–7335, 2011

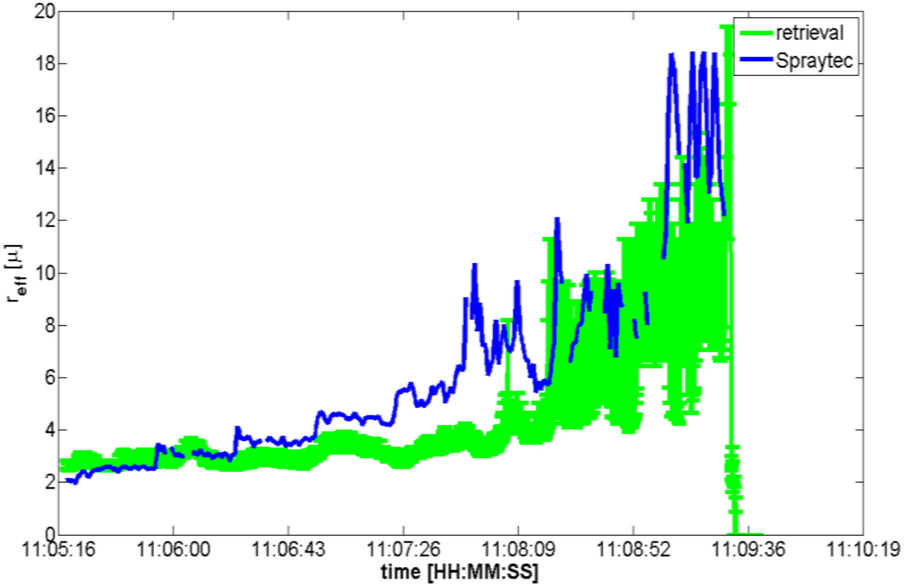

Fig. 23. Temporal effective radius of the artificial cloud which was sprayed during the controlled validation experiment. Blue: effective radius measured by the Spraytec. Green: effective radius retrieved by the proposed methodology. The range of the retrieved effective radius is the result of allowing 10 valid solutions (see stage (G) in Sect. 4).

AMTD
4, 7277–7335, 2011

Optical and microphysical properties of thin warm clouds

E. Hirsch et al.

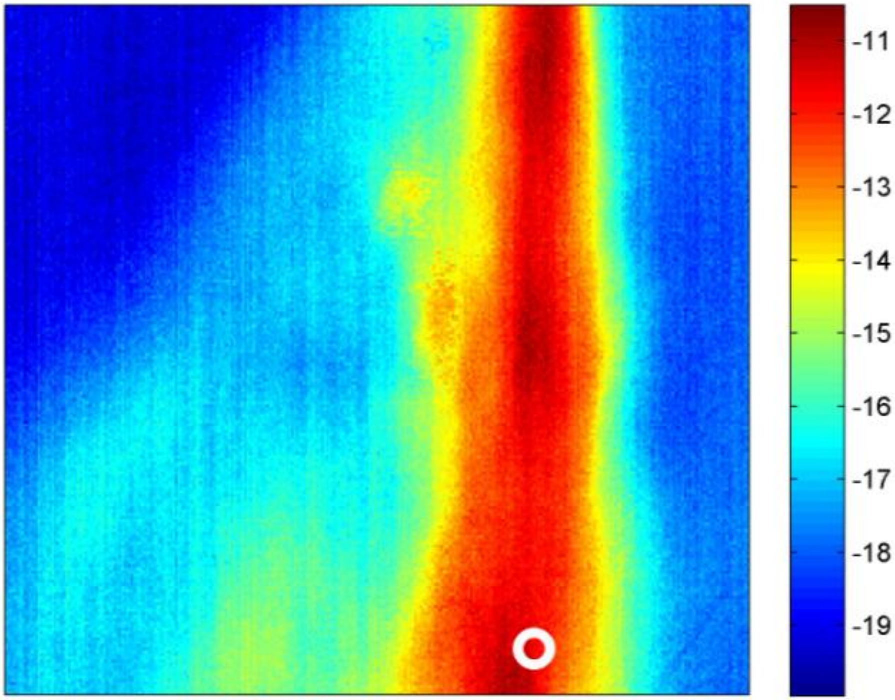

Fig. 24. A thermal image of the zenith sky (units in °C) during the validation experiment. The passing artificial cloud emerges from the nozzle which is located at the upper side of the image (not shown), and enters the field of view of the Spraytec, which is located at the lower side of the image (not shown). As expected, the passing cloud appears warm over the cold sky background. The white circle is the estimated position of the SR5000's field of view. Since the artificial cloud is relatively narrow, the apparent cloud in the SR5000's field of view is highly sensitive to fluctuations in the wind direction.

AMTD
4, 7277–7335, 2011

Optical and microphysical properties of thin warm clouds

E. Hirsch et al.